Geomorphological evolution of the Nile valley in relation to the Messinian Crisis

Masterarbeit
von
Christoph Pucher, BSc

Vorgelegt zur Erlangung des
akademischen Grades eines Masters of Science
der Studienrichtung Erdwissenschaften

Graz, im März 2018

Betreuer der Masterarbeit:
Kurt Stüwe

Eid (Ehrenwörtliche Erklärung)

Ich erkläre an Eides Statt, dass ich die vorliegende Arbeit selbstständig und ohne fremde Hilfe verfasst, andere als die angegebenen Quellen nicht benutzt und die den benutzten Quellen wörtlich und inhaltlich entnommenen Stellen als solche kenntlich gemacht habe.

Ich versichere, dass ich dieses Masterarbeitsthema bisher weder im In- noch im Ausland (einer Beurteilerin oder einem Beurteiler) in irgendeiner Form als Prüfungsarbeit vorgelegt habe.

Graz, im März 2018 .....

Abstract

The Messinian Crisis in the late Miocene (5.97-5.33 Ma) was caused by gradual restriction of the marine connection between the Mediterranean and the Atlantic due to tectonic processes at the Strait of Gibraltar. The period of the crisis comprises the onset of evaporitic conditions in the Mediterranean, a consequent sea-level fall of at least 1500 m and ends with the sudden refilling of the Mediterranean in the Zanclean. The sea-level fall had dramatic consequences for the rivers draining into the Mediterranean (e.g. Nile, Po, Rhone) as they had to adjust to their new base-level. Gigantic knickpoints formed at the mouth of the rivers and started to migrate upstream. This incision process formed canyons, some with dimensions comparable to the Grand Canyon of today. Collapse of the Gibraltar sill at the end of the Messinian Crisis led to abrupt refilling of the Mediterranean, its transgression into the canyons and their preservation due to their filling with Pliocene sediment. This study will focus on possibly the most impressive of these preserved canyons, the Messinian Nile canyon. The Messinian Nile canyon reached depths of 1500 m at Cairo and reached up to Aswan, some 1000 km further upstream. Given the short time-span of the sea-level low-stand (90-300 Kyr) makes this knickpoint one of the fastest migrating knickpoints in the world. Further, the canyon marks a river in transient conditions, as incision came to an end before a new steady-state could be obtained. Together with the large base-level fall, this makes it a great example for studying transient river evolution, as it allows the testing of different erosion models. These erosion models can produce identical steady-state river profiles, but show different behaviour during the transient evolution. Using OpenLEM, a landscape evolution model developed by Stefan Hergarten (University of Freiburg), different values for the slope exponent n of the routinely used stream-power family of erosion models and their influence on the river profile evolution were studied. This showed that a value of $n = 1$ as often assumed is not able to model the observed river profile evolution of the Messinian Nile. A detachment-limited stream-power model with a value of $n = 0.75$ was able to produce the expected incision at Cairo, Assiut and Aswan and is thus suitable for modelling the transient evolution of the Messinian Nile river.

Kurzfassung

Die Messinische Krise im späten Miozän (5.97-5.33 Ma) wurde durch tektonische Prozesse im Bereich der Meerenge von Gibraltar ausgelöst, die zur schrittweisen Einschränkung der marinen Verbindung zwischen dem Mittelmeer und dem Atlantischen Ozean führte. Der Zeitraum der Krise umfasst das Einsetzen von evaporitischen Bedingungen im Mittelmeer, sowie die daraus folgende Absenkung des Meeresspiegels um mindestens 1500 m und endete mit der raschen Wiederauffüllung des Mittelmeers im Zanklium. Die Absenkung des Meeresspiegels hatte dramatischen Folgen für die im Mittelmeer mündenden Flüsse (z.B. Nil, Po, Rhone). Diese mussten sich an das neue Meeresniveau anpassen. Gigantische Knickpunkte bildeten sich an den Flussmündungen, wanderten landeinwärts und gruben Canyons, deren Dimensionen teilweise mit denen des heutigen Grand Canyons vergleichbar sind. Zusammenbruch der Gibraltarschwelle am Ende der Messinischen Krise führte zur raschen Wiederauffüllung des Mittelmeers. Die Canyons wurden geflutet, mit Sedimenten des Pliozäns gefüllt und dadurch erhalten. Der vielleicht beeindruckendste dieser erhaltenen Canyons ist der Canyon des Messinischen Nils, welcher Thema dieser Arbeit ist. Der Canyon des Messinischen Nils erreichte eine Tiefe von 1500 m bei Kairo und reichte weitere 1000 km landeinwärts bis nach Aswan. Die relativ kurze Zeitspanne des Meeresspiegeltiefstandes (90-300 Kyr) macht den damit assoziierten Knickpunkt zu einem der sich am schnellsten fortbewegenden Knickpunkte der Welt. Da die Einschneidung des Canyons zu einem Ende kam, bevor sich ein neues Gleichgewicht einstellen konnte, beschreibt der Canyon außerdem einen Fluss, der sich nicht im Gleichgewicht befindet. Dadurch eignet er sich um verschiedene Erosionsmodelle zu testen. OpenLEM, ein von Stefan Hergarten (Universität Freiburg) entwickeltes Landschaftsentwicklungsmodell, wurde verwendet um für das routinemäßig eingesetzte stream-power Erosionsmodell die Auswirkung von verschiedenen Werten des Steigungs-Exponenten n auf die Entwicklung von Flussprofilen zu testen. Es konnte gezeigt werden, dass der oft angenommene Wert von $n = 1$ nicht für die Modellierung der Entwicklung des Messinischen Nils geeignet ist. Ein stream-power Erosionsmodell mit $n = 0.75$ konnte die zu erwartenden Erosionstiefen bei Kairo, Assiut und Aswan erreichen und eignet sich damit um die Entwicklung des Messinischen Niles zu beschreiben.

Contents

1. Introduction

The Messinian Salinity Crisis (MSC) or Messinian Crisis is an ecological crisis, starting with the onset of evaporitic conditions in the Mediterranean at 5.97 Ma, subsequent desiccation of the Mediterranean and ending with the reflooding of the Mediterranean at 5.33 Ma (Roveri et al., 2014). Evaporitic conditions were established by the gradual restriction of the marine connection to the Atlantic Ocean due to tectonic uplift processes in the gateway area leading to the gradual closing of the Strait of Gibraltar (Fig. 1). In further consequence the sea-level dropped at least 1500 m and the Mediterranean transformed into a giant evaporitic pool and finally into a brackish-water lake (Roveri et al., 2014). While this transformation had major ecological consequences, this study will focus on the impact of the dramatic sea-level lowering on the geomorphic evolution of the major rivers draining into the Mediterranean, in particular the Nile river. While the exact nature, amplitude, and timing of this sea-level fall is still debated (Roveri et al., 2014), it forced deep incision of long canyons and valleys such as Nile, Po and Rhone, as the rivers adjusted to

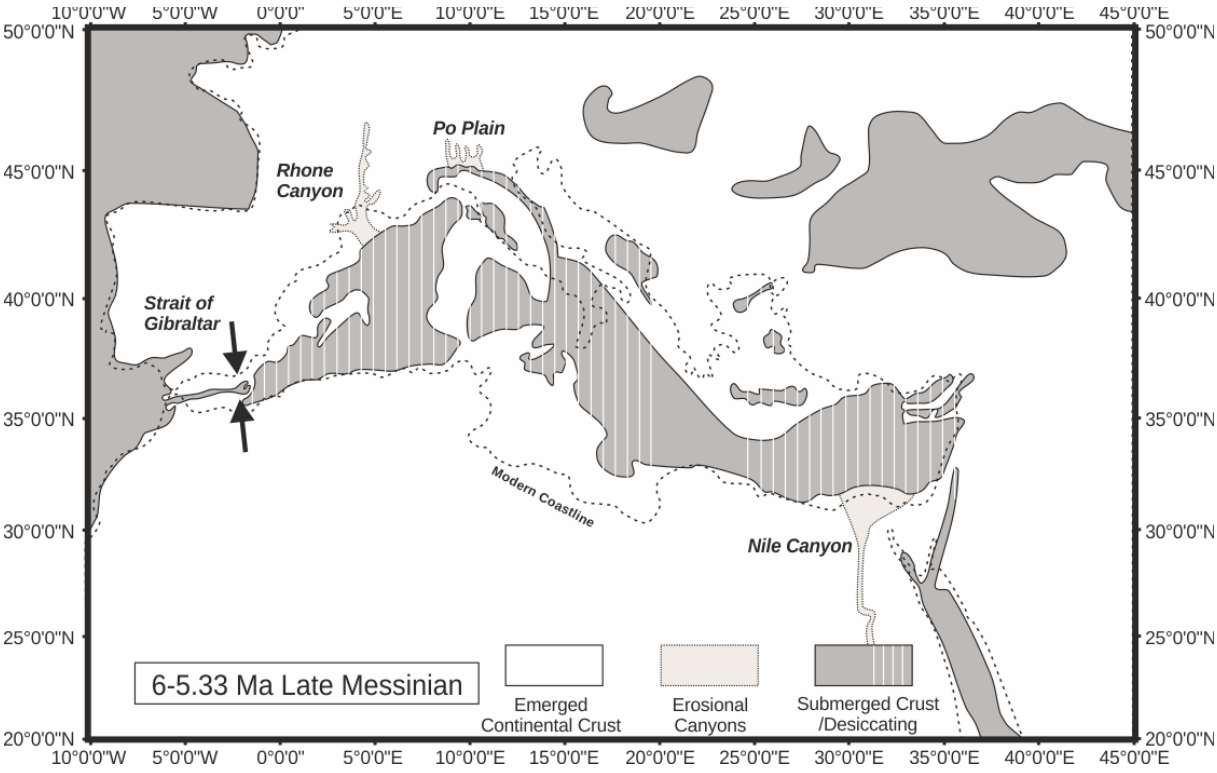

Figure 1: Paleogeographic setting of the Mediterranean during late Messinian time. Shown are the partly desiccated Mediterranean and the Messinian erosional canyons of the Po plain and Nile and Rhone rivers. The arrows indicate the closure of the Strait of Gibraltar. (modified after Jolivet et al., 2006)

their new base-level (Fig. 1). Abrupt collapse of the Gibraltar sill led to the reflooding of the Mediterranean at 5.33 Ma and can be seen as an instantaneous event in geological terms (Roveri et al., 2014; Hsue et al., 1973). The catastrophic flood caused the very rapid rise in sea-level up to 80 m above the present day sea-level and the refilling of the Messinian canyons by mass deposition of the suspended load of the Messinian rivers (Loget and Van Den Driessche, 2009). These deposits inhibited the erosion of rivers and consequently the morphology of the Messinian canyons is largely preserved (Loget and Van Den Driessche, 2009).

The Messinian Nile Canyon cut by a predecessor of the modern Nile river, the Eonile river, was approximately 12 km wide and at least 1.5 km deep beneath Cairo (Barber, 1981). This suggests a base-level fall of at least 1500 m in the Mediterranean, forming dramatic knickpoints in the major rivers draining into the Mediterranean. The resulting increased erosive power of the Nile river and the timedepent migration of the formed knickpoint along the Nile channel will be the main topic of this thesis. The migration of the knickpoint cut the Nile Canyon up to Aswan and came to an abrupt end by the refilling of the Mediterranean. Given the relatively short time span of the Messinian Crisis, or the even shorter time span from the desiccation of the Mediterranean to its refilling, makes this knickpoint one of the fastest migrating knickpoints in the world. Moreover, due to the sea-level rise at the end of the MSC, incision came to an abrupt end due to the refilling of the canyon by Pliocene sediments. Thus the preserved Messinian Nile canyon marks a river in transient state, which makes it a great example for the study of transient river evolution.

2. Messinian Salinity Crisis

The end of the Miocene marks a time of great transformation in the Mediterranean realm as the marine connection of the Mediterranean to the Atlantic was gradually restricted. This turning of a small ocean into a brackish-water lake is known as the Messinian Salinity Crisis (MSC) (Roveri et al., 2014).

Gradual restriction of the marine connection between the Mediterranean and the Atlantic is thought to be the consequence of tectonic uplift processes in the gateway area, which can be explained by lithospheric slab detachment and roll back processes underneath the Gibraltar Arc (Duggen et al., 2003; Garcia-Castellanos and Villaseñor, 2011; Roveri et al., 2014). This restriction induced a sea-level fall in the Mediterranean and the deposition of up to 2000 m of evaporites (Hsu and Cita, 1973). The amplitude and precise magnitude of local sea-level fall during this period as well as the timing and nature (one or more steps) are still subject to debate (Gargani et al., 2014; Roveri et al., 2014).

This thesis will adopt the deep-basin shallow-water hypothesis which implies the desiccation of the Mediterranean (Hsu and Cita, 1973) and its transformation into a giant salt desert more than 1000 m below global sea-level (Roveri et al., 2014). This scenario is supported by deep canyons that formed by major incision of pre-MSC drainage networks all around the Mediterranean realm, such as the Nile, Rhone and Po rivers (Fig. 1; Chumakov, 1973; Barber, 1981; Clauzon, 1978; Loget et al., 2005; Bini et al., 1978). These rejuvenation of the rivers draining into the Mediterranean are thought to be the consequence of a major sea-level fall forcing the rivers to adjust to their new base-level. For the Nile and Rhone rivers the Messinian canyons underlie their current valleys. In the case of the Po plain, Messinian canyons can be traced on the subsurface but can also be seen on the surface in form of the south Alpine lakes (Maggiore, Como, Iseo and Garda) (Bini et al., 1978; Finckh, 1978). These narrow, in a north-south direction elongated lakes with floors that lie below modern sea-level are remnants of the Messinian crisis (Bini et al., 1978). The lakes Maggiore, Como and Iseo are interpreted as former Messinian canyons deeply incised by their Messinian rivers (Ticino, Adda, Oglio respectively), while lake Garda is interpreted as a deep depression formed by erosion of the Alpine margin along the Garda embayment (Bini et al., 1978).

A 3-stage stratigraphic model for the MSC has been proposed by CIESM (Commission Internationale pour l'Exploration Scientifique de la mer Méditerranée) (Gaullier et al., 2008; Roveri et al., 2014).

The first stage (5.97-5.6 Ma) marks the onset of the MSC and the first evaporitic stage. The beginning of the MSC has been defined by the transition to evaporitic conditions and the deposition of the lowermost gypsum bed at ~5.97 Ma (Roveri et al., 2014). No major sea-level drawdown is thought to have happened during that stage (Govers et al., 2009).

The second stage (5.6-5.55 Ma) includes the climax of the MSC and was dominated by thick primary halite and clastic gypsum deposits (Roveri et al., 2014). Within this stage the large sea-level drawdown took place. This led to widespread subaerial erosion and the development of the Messinian erosional surface and Messinian canyons (Roveri et al., 2014).

During the third stage (5.55-5.33 Ma) precipitation of selenite and cumulate gypsum facies in shallow-water sub-basins in southern and eastern areas, and deposition of evaporite-free clastic deposits in the northern and western areas dominate (Roveri et al., 2014). In this time the Mediterranean basin underwent substantial paleogeographic and paleoclimatic modifications with important hydrological consequences and there is evidence for Mediterranean exchange with other water masses (e.g. Atlantic and Paratethys) (Roveri et al., 2014). These intra-basinal connections and water exchanges are also consistent with the assumption of a relative base-level rise throughout the Mediterranean during this stage (Roveri et al., 2014).

The end of the MSC is marked by the sudden refilling of the Mediterranean and the return to fully and stable marine conditions throughout the Mediterranean realm (Roveri et al., 2014). This event, termed the Zanclean flooding (5.33 Ma), is thought to be a geologically instantaneous event and implies the abrupt collapse of the Gibraltar sill and the consequent catastrophic flood of Atlantic waters into the Mediterranean basin (Roveri et al., 2014). The sea-level rose up to 80 m above present day sea-level which led to the flooding of the former carved canyons and their preservation due to their filling with Pliocene sediment (Loget and Van Den Driessche, 2009).

2.1. Messinian sea-level low-stand and associated Messinian canyons

Many Messinian canyons have been documented in the Mediterranean area, the Rhone canyon in the Western Mediterranean and the Nile canyon in the Eastern Mediterranean probably being the two most impressive ones (Fig. 1). Due to the Sicily sill, which may have disconnected the two basins at lower sea-level, the Western and Eastern Mediterranean could have experienced a different evolution during the MSC (Gargani et al., 2014). It is thought that the sea-level lowering was deeper in the Eastern Mediterranean basin than in the western basin (Gargani et al., 2014). This could be due to the Eastern Mediterranean having a larger excess evaporation and broader surface area over which evaporation took place compared to the west (Ryan, 2009).

The estimates of the magnitude of the sea-level fall are often based on the associated Messinian canyons. For the Western Mediterranean basin a sea-level fall in the order of ~1500 m is suggested, based on deep incision which is observed along the Ebro margin, in the Gulf of Lion and in the Valencia basin (Gargani et al., 2014). Clauzon (1982), using the magnitude of the incision of the Messinian Rhone canyon, estimated a sea-level drop of ~1600 m for the Western Mediterranean (Ryan, 2009).
For the Eastern Mediterranean seismic profiles showing erosional surfaces along the Egyptian margin were used to estimate a sea-level drop of 1500-2250 m (Gargani and Rigollet, 2007).

Gargani and Rigollet (2007) further argue that there was not one sea-level lowering but that numerous sea-level falls at various depths have happened in the Western as well as the Eastern Mediterranean basin. For the Western Mediterranean they suggest a two-phase sea-level lowering, as proposed by Clauzon et al. (1996), where water-level fluctuations may have occurred at ~-500 m, and then at ~-1500 m.
In the Eastern Mediterranean this would also allow the interpretation of the 3-5 phases of erosion observed on the Egyptian margin (Gargani and Rigollet, 2007).

Regarding the duration of the sea-level lowering, Gargani (2004) proposes 400 Kyr for the first phase and 50 Kyr for the second phase. Gargani et al. (2010) come to the conclusion that the duration of the sea-level main low-stand is probably less than 100 Kyr. This is in accordance with Krijgsman et al. (1999), who estimate a duration of ~90 Kyr (between 5.59 and 5.50 Ma) for the ‘Messinian gap’, which would also

coincide with the second stratigraphic stage of the MSC as suggested by the CIESM. Clauzon et al. (1996) suggest the period of 5.60 to 5.32 Ma (~ 300 Kyr) for the cutting of the Messinian canyons, which comprises the second and third stratigraphic stages of the CIESM model.

2.2. Climate in northeastern Africa during the MSC

Globally the climate is thought to have been warmer and wetter in the Late Miocene than it is today (Zachos et al., 2001, 2008). Simulation of the Late Miocene Mediterranean hydrological budged shows that net precipitation (precipitation minus evaporation) across most of the Mediterranean region is similar to present day, with evaporation exceeding precipitation particularly strongly in the Eastern Mediterranean basin (Gladstone et al., 2007). A significant difference does occur in North Africa where the modelled net precipitation (and both precipitation and evaporative water loss separately) is much higher in the Late Miocene compared to today (Gladstone et al., 2007). The region of increased net precipitation in North Africa coincides with ancient Messinian river catchments that drained north into the Mediterranean, but are dry today due to low rainfall (Gladstone et al., 2007). This is in accordance with Griffin (2002) who also proposes a wet climate in North Africa during the Late Miocene. Amongst other evidence he came to this conclusion by comparing the Messinian incision of three main rivers of North Africa that drained into the Mediterranean during the Late Miocene. These three main rivers are the Eonile (a pre-stage to the current Nile drainage system, responsible for the cutting of the Nile canyon as will be discussed later; Said, 1981), the Eosahabi and the Gabes, with the Nile drainage system being the only one still active today. All three rivers incised into bedrock during the MSC but to different degrees, with the Eonile being by far the most deeply incised (Griffin, 2002). As all three rivers experienced the same magnitude of base-level fall, the difference in incision can be accounted by different discharge, related to drainage area and rainfall intensity (Griffin, 2002). The comparison by Griffin (2002) is based on the assumption that fluvial energy, which is reflected in the degree of incision, is mainly related to rainfall because elevation, in this case, is principally a product of base-level fall (Griffin, 2002). Taking drainage area into account and comparing the three river networks a profile with southeasterly and easterly increase in rainfall can be reconstructed (Griffin, 2002). This indicates that northeastern North Africa was the most humid of these three areas during the Messinian (Griffin, 2002).

Griffin (2002) explains this by the northward migration of the Inter-Tropical Convergence Zone (ITCZ), the zone in which the easterlies from each hemisphere converge and ascend releasing abundant moisture on the land or sea below. During the Tortonian arid conditions prevailed in northeastern Africa (Griffin, 1999). Transition to a wetter climate in the Messinian is reflected in the rapid deposition of the Zeit Formation, as well as in its high siliciclastic content (Griffin, 1999). Griffin (1999) states that an increase in rainfall would lead to an increase in sediment carrying capacity so that precipitation is positively correlated with denudation rate which allows for the assumption that the Zeit Formation reflects wetter conditions. The Zeit Wet Phase (from ~7.5 to 5 Ma) is then a period of humid northeastern Africa during the Messinian, as an expression of the initiation and early evolution of the Asian monsoon and its impact on the African monsoon and associated desert system (Griffin, 2002). The Asian monsoon initiated in the late Tortonian about 8 Ma in relation to significant uplift of Tibet and developed in two stages (Molnar et al., 1993). The first between about 8 and 4.6 Ma with more or less regular alternation between an Arabian Sea southwesterly monsoon (the SW monsoon) and an Arabian Sea southeasterly monsoon (the SE monsoon) (Griffin, 2002). The SW monsoon is thought to transport moisture away from northeastern Africa towards southern Asia, while the SE monsoon is more focused on North Africa (Griffin, 2002). Increase of the land area of subtropical North Africa in an area of the world that receives the maximum summer insolation due to the northwards migration of Africa would enhance the SE monsoon (Barry and Chorley, 2010; Griffin, 2002). The substantially dried Mediterranean being a focus of low pressure during the summer would then strengthen the Zeit Wet Phase and expand it further north, bringing moisture to the Mediterranean itself (Griffin, 2002). This makes it very likely that much of the moisture of the Zeit Wet Phase was monsoonal and derived from the Indian Ocean and not from the desiccated Mediterranean as was proposed by Said (1994) (Griffin, 2002). After the Zeit Wet Phase the Asian aspect of the monsoon (SW monsoon) became more dominant and in time the SE monsoon waned (Griffin, 2002). In general this led to more arid conditions during the Pleistocene, which was punctuated by episodes of increased local rainfall and led to the development of Egypt into a desert (Said, 1981). Today Egypt experiences hyperarid climate, which is regarded as a result of the northward drift of Africa in space and time (Abdelkareem et al., 2012).

3. The Nile

3.1. The modern Nile river in the Egyptian region

The modern Nile has a length of 6825 km from its sources near Lake Victoria in Tanzania, to the shores of the Mediterranean, draining an area close to 3,000,000 km² (Fig. 2; Said, 1981; Woodward et al., 2007). Compared to other modern rivers with similar drainage area its annual discharge of 86 billion $m^3\ yr^{-1}$ is quite low (Said, 1981). Generally it flows south to north, crossing 35 degrees of latitude, while its source in Equatorial Africa and its mouth in the Mediterranean lie within one degree on the same meridian of longitude (Said, 1981). On its course the Nile negotiates its way through five different regions which differ from each other in relief, texture, climate, geologic structure and history (Said, 1981). From south to north these are the Lake plateau, the Sudd and Central Sudan, the Ethiopian highlands, the cataracts and the Egyptian region (Said, 1981; Fig. 2 and 3). The focus will be on the Egyptian region as the course of the modern Nile river in the Egyptian region is closely related to the Messinian Nile canyon that has been cut during the MSC by the Eonile river (Said, 1981). Further, connection with the Ethiopian Plateau and Equatorial Africa seems to have only been established in the Pleistocene (Roden et al., 2011; Said, 1994).

In Egypt the Nile river has a length of ~1200 km and throughout this part of its course, the modern river receives not a single active tributary (Said, 1981). The Nile enters Egypt from the Sudan at Wadi Halfa (Said, 1981). It then flows for around 350 km within a narrow valley bordered by abrupt cliffs of sandstone and granite until it reaches the first cataract near Aswan (Said, 1981). The region between Wadi Halfa and Aswan is now completely drowned by the lake Nasser due to the construction of the Aswan High Dam across the river at the head of the cataract (Said, 1981).
The Aswan cataract, as well as the cataracts further upstream, are due to outcrops of Precambrian crystalline rocks which offer far greater resistance to erosion by the river than the Nubia sandstones (Mesozoic sedimentary rocks) of the intervening stretches (Said, 1981; Fig. 2). The exposure of these Precambrian crystalline rocks around the city of Aswan is thought to be the result of uplift associated with the Nubian Swell (Roden et al., 2011; Thurmond et al., 2004). Downstream of the Aswan cataract, the valley begins to broaden, reaching the Silsila gorge bound on both sides by quartizitic

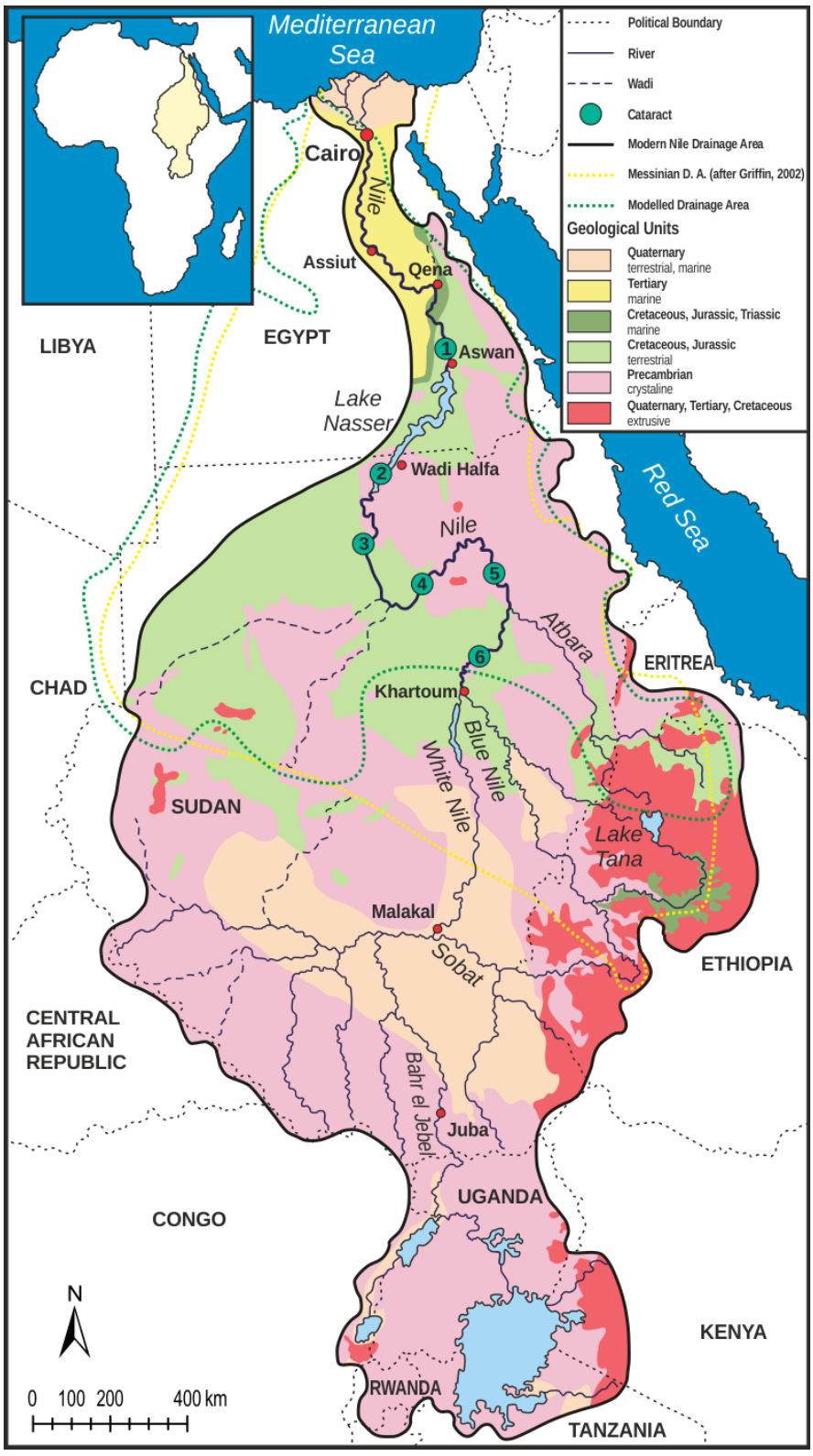

Figure 2: The modern Nile river and its modern drainage basin. Messinian drainage basin as suggested by Griffin (2002) is shown by the green dotted line. Modelled drainage basins (yellow dotted line) corresponds to a possible Messinian drainage area that was used for modelling the evolution of the Messinian Nile river (see text for further explanation). (modified after Woodward et al., 2007)

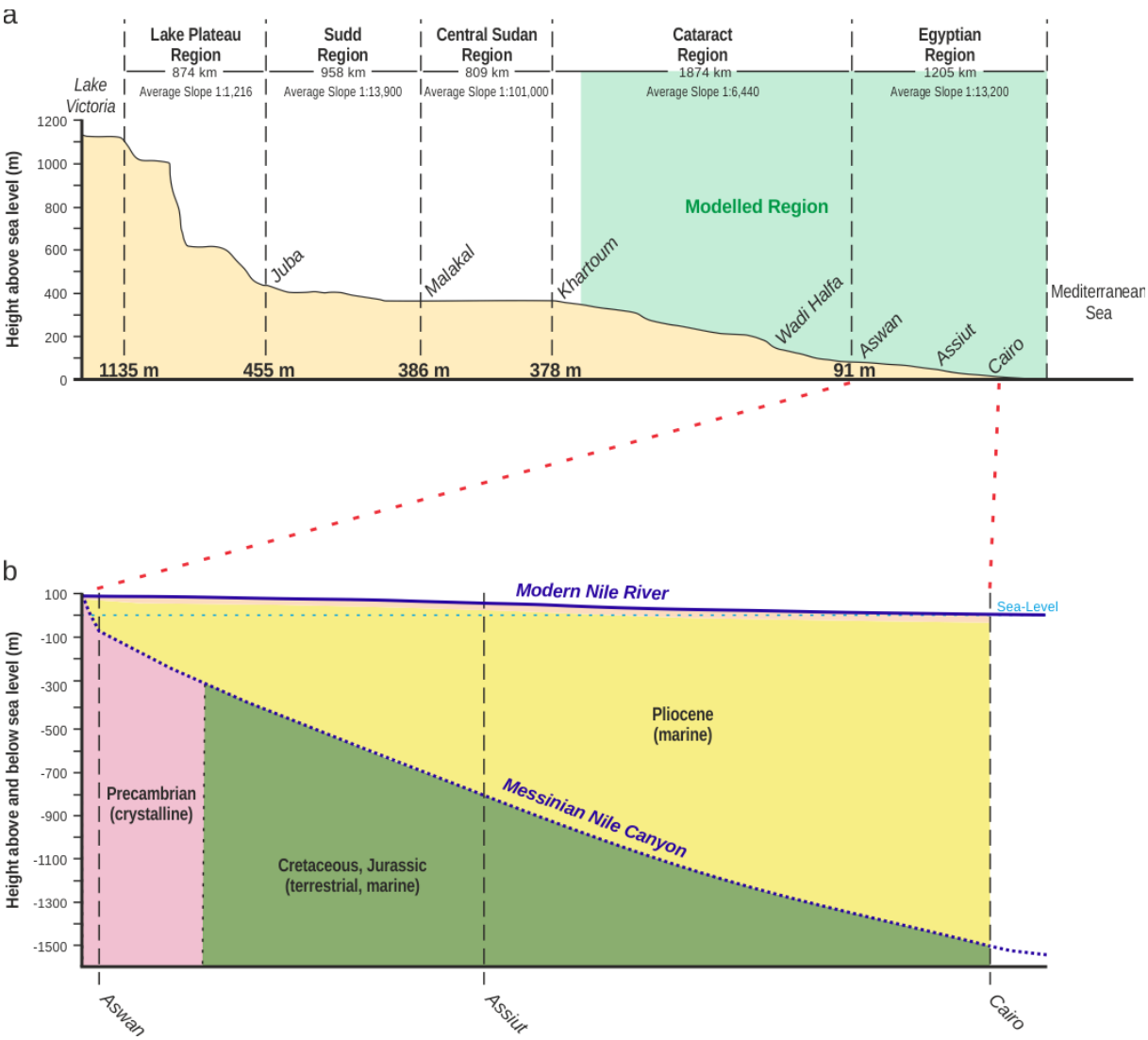

Figure 3: (a) Longitudinal profile of the modern Nile river. Modelled region corresponds to the modelled drainage area as seen in Fig. 2. Locations of cities can also be seen in Fig. 2. (b) Enlargement of the river profile between Aswan and Cairo. This corresponds to the path of the modern Nile river influenced by the Messinian incision. Possible longitudinal profile of the Messinian Nile canyon is also shown, based on the assumed incision at Cairo (-1500 m), Assiut (-800 m) and Aswan (~-100 m) (see text for further explanation). (modified after Woodward et al., 2007)

sandstone of the Nubia sandstone 60 km to the north of Aswan (Said, 1981). About 160 km downstream of Aswan, near Esna, this sandstone of the bounding cliff is replaced by limestone (Said, 1981). Further 120 km downstream at Qena the river makes a great bend with limestone cliffs rising to heights of more than 300 m on either side (Said, 1981). After the Qena bend, the Nile directs its way to the Red Sea and the valley broadens markedly (Said, 1981). Near Assiut, some 260 km downstream of Qena, the cliffs on the western side become much lower than those on the east (Said, 1981). This continues for around 400 km to Cairo (Said, 1981).

South of Cairo the delta, beyond its apex, spreads in a plain studded with an intricate network of canals and drains (Said, 1981). The modern delta tributaries are the western Rosetta branch, about 239 km long, and the eastern Damietta, about 6 km longer (Said, 1981).
The gradient of the Nile within the Egyptian region is immensely gentle, with Aswan, almost 1000 km from the sea, lying only 91 m above present sea-level (Fig. 3a; Woodward et al., 2007).

3.2. Evolution of the Nile system and the cutting of the Messinian Nile canyon

The earliest river associated with the Nile drainage system as known today is the Eonile river, responsible for the cutting of the Messinian Nile Canyon (Said, 1981). Earlier, pre-late Miocene rivers which drained the elevated lands of Egypt do not seem to have been associated with the valley in its present form (Said, 1981). Issawi and McCauley (1992) propose two major drainage systems prior the Nile system, termed the Gilf system and the Qena system (Fig. 4a; Roden et al., 2011).

The Gilf system consisted of a northward flowing consequent stream that followed the Tethys Sea as it retreated, creating newly emerged land in Egypt (Goudie, 2005). It also consisted of some streams that formed on the flanks of the Red Sea region towards the end of the Eocene (Goudie, 2005). The Qena system was caused by major tectonic activity in the Red Sea area, causing reversal of drainage to occur with a large river flowing southwards towards Aswan and the Sudan (Goudie, 2005). The south-trending Wadi Qena originates from this time (Goudie, 2005).
The river directly preceding the Eonile river, herein termed pre-Nile river, was not part of these two river systems. According to Said (1981) the pre-Nile river followed a northwesterly course from Assiut, traversing the Western Desert and debouching at the eastern tip of the Qattara depression (El Bahr river in Fig. 4a; Said, 1981). Middle Miocene normal faulting parallel to the Red Sea rift shifted this rivers fluvio-delta system from this earlier position in the Western Desert to approximately its present location (El Mahmoudi and Gabr, 2009). The sea-level lowering during the MSC then led to headward erosion and cutting of the Nile canyon by the pre-Nile river and subsequent capturing of the Qena system due to gradient advantage (Goudie, 2005). The connected Eonile river system became the first that extended the length of Egypt to the Mediterranean (Fig. 4b; Goudie, 2005).

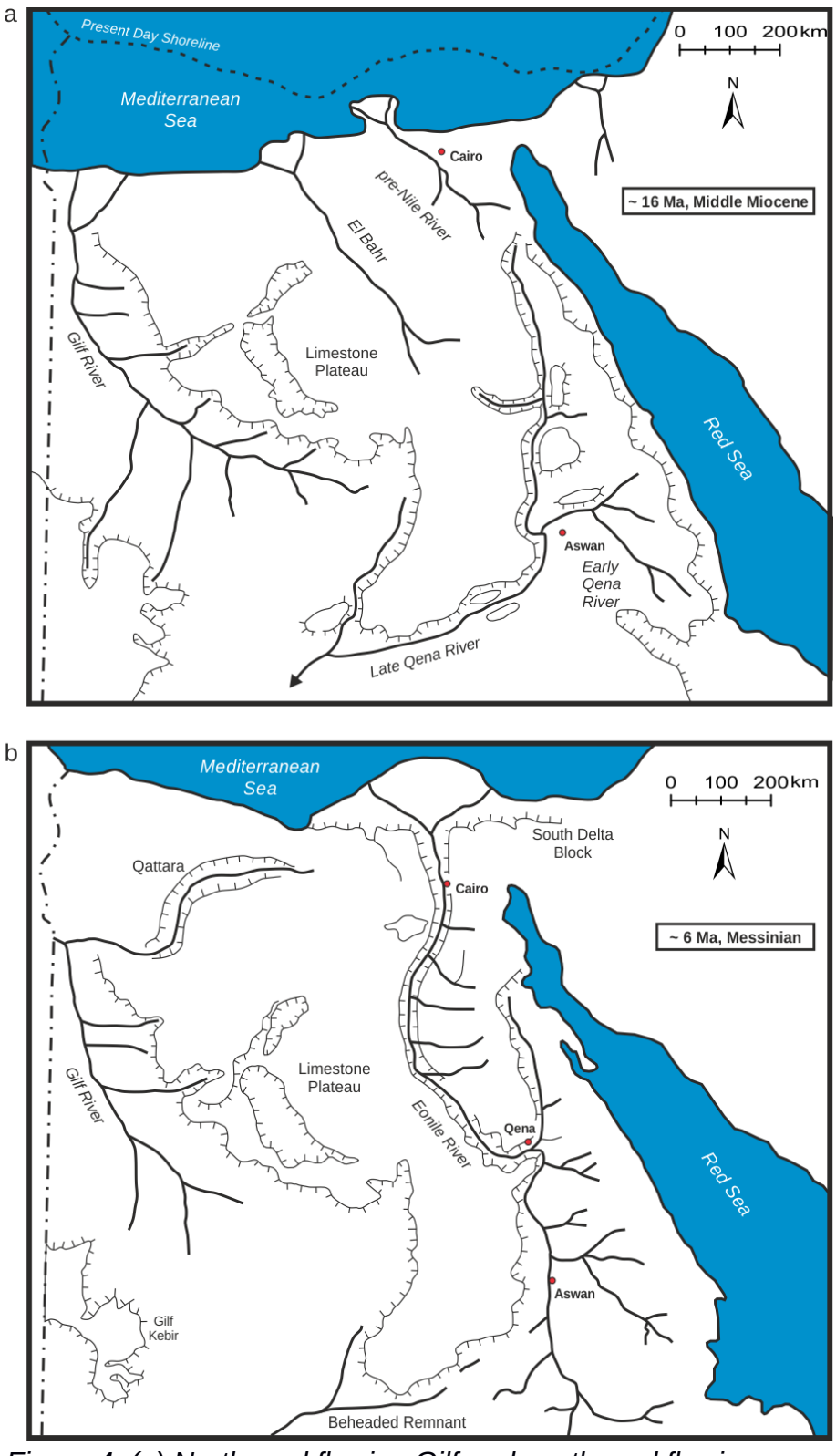

Figure 4: (a) Northward flowing Gilf and southward flowing Qena river systems that drained Egypt prior to the Nile system. Two possible predecessors of the Eonile river are shown (El Bahr river and pre-Nile river) (b) Eonile river of the Nile system, after the pre-Nile river (preceding the Eonile) caugth the Qena river (see text for further explanation). (modified after Goudie, 2005)

The Eonile river cut its canyon as far inland as Aswan, lying about 1000 km upstream the present coastline (Fig. 2 and 3; Barber, 1981). Beneath the modern city of Cairo, it had cut a ‘V’-shaped gorge down through sandstone, basalt and limestone that was approximately 12 km wide and at least 1.5 km deep (Ryan, 2009; Barber, 1981). The depth of the canyon reached 800 m at Assiut decreasing to around 150 m at Aswan (Fig. 3b; Said, 1981; Chumakov, 1973). Paired and impaired rejuvenation terraces, as observed by Barber (1981), suggest constant lowering of base-level, with dramatic falls related to sudden changes in Messinian sea-level.

The Eonile river seems to have cut its channel in the elevated north Egyptian plateau passing through the South Delta block and cascading over the hinge zone until it fanned into the North Delta embayment depositing its load in a series of coalescing fans (Fig. 4b; Said, 1981). Most of the sediment transported by the Eonile came from the Cretaceous and Eocene carbonates (Said, 1981; Barber, 1981). However, in the South Delta block the Eonile canyon cut through a thick basalt sheet and Oligocene sand and gravel beds before it cut the Eocene, Cretaceous, and finally the Jurassic rocks which most likely made the bottom of the canyon (Said, 1981). Same as the Colorado river today, the Eonile canyon cut its path in bare horizontally disposed sedimentary strata varying in lithology (Said, 1981). It probably resembled the Grand Canyon of the Colorado river today, although the Eonile canyon seem to have been longer and deeper, with approximately the same width as the Colorado canyon (Said, 1981). The Eonile had a much higher gradient between present day coastline and Aswan compared to today (Said, 1981).

The path of the Eonile canyon coincides with a seismic belt, which is in agreement with the view that the path of the Eonile was originally determined by tectonics and was then eroded by the river (Said, 1981). The Nile valley can be interpreted as a large elongated Oligo-Miocene rift, trending N-S as an echo of the Red Sea rifting, which may also have been responsible for changing the course of the river preceding the Eonile (El-Sayed et al., 2004). Its during this Oligocene and Miocene times that the structure of northern Egypt evolved and has remained since then almost inactive except for minor tremors and earthquakes along some of the older lines (Said, 1981).

Marine ingression into the excavated canyon of the Eonile was caused by the Zanclean flooding (5.33 Ma), the sudden refilling of the Mediterranean basin at the end of the MSC by abrupt collapse of the Gibraltar sill (Roveri et al., 2014). The rising

of the sea-level up to 80 m above present day sea-level brought the Mediterranean into the Nile valley depression transforming it into a narrow long gulf reaching as far south as Aswan (Said, 1981). Marine sediments of the early Pliocene filled about one third of the depth of the ancient Eonile canyon (Said, 1981). The gulf was converted into a channel by the Paleonile of the late Pliocene that succeeded the Eonile river (Said, 1981). The canyon was completely filled up by the end of the Paleonile sedimentation (Said, 1981; Zaki, 2007). After the Eonile and Paleonile systems the Nile system went through three more episodes of evolution (Protonile, Prenile, Neonile), with the Neonile system being still active today (Said, 1981). These episodes of the Nile system are not discussed in this thesis and interested readers are pointed to Said (1981).

Regarding the drainage area of the Eonile river, Griffin (2002) suggest that during the Messinian most of the water of the Eonile river was derived from Egypt itself (Said, 1994) and probably northern Sudan, which is consistent with the assumption that Egypt during Late Miocene time experienced a wet climate with heavy rainfalls. This is in strong contrast to today, as Egypt today lies within the Sahara desert and the Nile river gets its waters from sources outside Egypt, receiving not a single active tributary within the Egyptian borders (Said, 1981). Griffin (2002) estimates the drainage area to be approximately 2,100,000 km². He interprets the Eonile basin as the part of the Nile drainage basin north of the Sudd area and southern Sudan, also including parts of the Ethiopian Highlands which may only have been connected to the Nile river system in Pleistocene times (Fig. 2; Griffin, 2002; Roden et al., 2011). The a priori assumption that pre-MSC drainage areas was similar to present-day drainage areas, as made by Loget et al. (2005) in their quantification of Messinian knickpoint migration rates, does not seem adequate for the Nile river, as climate and the river network (connection with Equatorial Africa and Ethiopian Highlands) seem to have been fundamentally different in Messinian times. Also the assumption made by Abotalib and Mohamed (2013), that connection of the northward flowing predecessor of the Eonile (they termed the North Egypt River System) and the Qena system was established only after marine ingression in the Pliocene will also be disregarded, as it does not seem likely that a river only reaching up to approximately Assiut would have enough power to cut the Messinian Nile canyon as observed.

4. Fluvial geomorphology

Cutting of the Messinian canyon by the Eonile river is clearly dominated by fluvial processes. River incision into their bedrock is a critical process for landscape evolution and also one way how rivers can react to transient conditions caused by changes in boundary conditions (e.g. base-level), so that a new steady-state can be obtained. Changes in base-level, as in the case of the Messinian Nile river, will often take the form of knickpoints. These knickpoints then migrate through the river network, communicating the changes of downstream boundary conditions and lowering the rivers bedrock as they move upstream. The next sections deal with these topics (river incision, rivers in steady-state and transient condition, knickpoints). To do this, one has to classify different channels and their respective characteristics, as they have different river incision mechanisms and therefore react differently to changes.

4.1. Channel classification

Howard et al. (1994) and Howard (1998) identify five major channel types, differing in morphology, dominant processes and timescales of adjustment, which more generally can be merged into two types: bedrock and alluvial channels.

Alluvial channels have a coherent (in space and time) blanket of transportable sediment on both the bed and banks (Whipple and Tucker, 2002). In live bed conditions the channel gradient is primarily set by sediment flux, whereas in threshold conditions it is primarily set by the critical shear stress for the initiation of motion (Whipple and Tucker, 2002). Alluvial channels do not actively incise into their bedrock but can change their slope by aggradation and degradation of sediment particles.

Bedrock channels do not have a coherent blanket of transportable sediment. But they are not characterized by channels where bed and banks are largely composed of in-place rock either, as the term bedrock channel would imply (Whipple et al., 2013). Most of the length of so called bedrock rivers is in fact covered with thin and patchy sediment cover and rock outcrops may be rare (Whipple et al., 2013). This led Howard (1994) to the introduction of the term mixed bedrock-alluvial channels. While this should be kept in mind, the term bedrock river is still valid, considering that although covered with a thin sediment cover, rock is everywhere close to the surface, so that bedrock rivers are commonly incising through in-place rock (Whipple et al.,

2013). This is what makes bedrock rivers special and why they play a critical role in landscape evolution. Whipple et al. (2013) defined bedrock rivers by satisfying either one or both of the following two conditions: (1) the long-term capacity of the river to transport bedload is higher than the long-term supply of bedload, so that in general sediment-starved conditions dominate and rock is exposed in bed and banks with only thin, patchy, and temporary alluvial cover (Montgomery et al., 1996); or (2) the river is actively incising through in place rock over the long-term (millennial to geologic timescales).

River channels can also be classified in a similar way on the basis of their dynamics, of what factors govern the rate of channel incision (Whipple and Tucker, 2002). This rate of channel incision can be limited either by the ability of the rock to detach particles (as on strongly cohesive or indurated substrate) termed detachment-limited or by the ability of the flow to transport particles (as on a bed of loose, non-cohesive sediment) termed transport-limited (Tucker and Hancock, 2010).

In *transport-limited* systems the rate of incision is set by the downstream divergence of sediment transport capacity, so that river incision only occurs if the local transport capacity of the stream is greater than the sediment load supplied from upstream (Whipple and Tucker, 2002). In *detachment-limited* systems the rate of incision is determined by the stream's ability to erode the bed (Whipple and Tucker, 2002).

As Whipple and Tucker (2002) point out, under constant environmental conditions there should be in general a simple correspondence between the two mentioned classification schemes. So that a live bed alluvial channel should also be transport-limited and a bedrock channel close to detachment-limited. But they also state that, as bed morphology can change quickly in response to new conditions, channel morphology at any one time is not necessarily a reliable indicator of long-term behaviour. Therefore, for the analysis of long-term behaviour, the behavioural channel classification (detachment-limited, transport-limited and hybrid) is better suited.

4.2. Fluvial erosion

Flowing water erodes bed by detaching the particles from the bed and carrying them downstream (Tucker and Hancock, 2010). The rate of erosion under a water current can then be either detachment-limited or transport-limited as introduced above

(Tucker and Hancock, 2010). As the Messinian Nile river actively incised into its bedrock and thereby cut its canyon, this thesis will focus on detachment-limited systems. For the purpose of modelling fluvial erosion the landscape evolution model (LEM) OpenLEM developed by Stefan Hergarten (University of Freiburg) will be used. OpenLEM allows to model fluvial erosion, sedimentation, diffusive erosion, flexural isostasy and landslides. Although probably all of these mechanism were active during the cutting of the Messinian canyon only fluvial erosion as the primary mechanism will be modelled. OpenLEM implements fluvial erosion by by the stream-power erosion model in the form of a detachment-limited erosion model.

4.2.1. Detachment-limited

A detachment-limited system can be pictured as described by Tucker and Hancock (2010): Consider a channel formed in highly cohesive clay sediment, in which individual small particles are glued together. If the force exerted on the bed by the flowing water exceeds the cohesive strength that binds a grain or aggregate to its neighbour, the particle will be detached. If these particles are ‘hydraulically small’ they tend to remain suspended in the water column until and unless the flow slackens considerably. Thus, if one is interested only in the erosional part of the system – and assuming that the sediment concentration does not grow so large that the flow becomes hyperconcentrated – the ultimate settling of the particle can be ignored (Tucker and Hancock, 2010). Thus, a detachment-limited model (Howard and Kerby, 1983; Howard, 1994) is one in which particles effectively disappear as soon as they are eroded, leading to the continuity of mass equation:

$$\frac{\partial h}{\partial t} = B - E \tag{1}$$

where h is surface height, t is time, E is the erosion rate in depth per time, and B being a source term (such as uplift or subsidence relative to a given base-level) (Tucker and Hancock, 2010). As suggested by Howard and Kerby (1983), E depends on bed shear stress τ and adding a critical threshold of bedload motion τ_{cr} that must be exceeded for erosion to occur, bed erosion rate E can be formulated as (Whipple et al., 2013):

$$E = k_e f\left(q_s\right)\left[1 - \left(\tau_{cr}^{a} / \tau^{a}\right)\right]\tau^{a} \tag{2}$$

Where k_e is a function of substrate properties (large values for weak, easily eroded materials), $f(q_s)$ describes the influence of the tools and cover effect of sediment (Sklar and Dietrich, 2004), and the exponent a depends on the mechanics of erosion. If the threshold stress is negligible for the floods of interests, then the term in the brackets vanishes (Whipple et al., 2013).

Equation 2 can be reformulated using empirical relations for hydraulic geometry, basin hydrology and assuming conditions of steady, uniform flow (Kirby and Whipple, 2012). A generalized form of the stream-power family of erosion models can then be written as (Whipple and Tucker, 1999; Whipple et al., 2013),

$$E = K A^m S^n \tag{3}$$

where K is the erosion coefficient (or erodibility), A is drainage area as a proxy for discharge, S is bed slope and m and n are area exponent and slope exponent respectively.

Coupling equation (3) with the detachment-limited mass balance (Eq. 1), and substituting the source term B with uplift rate U, one gets:

$$\frac{\partial h}{\partial t} = U - E = U - K A^m S^n \tag{4}$$

An equation in the form of equation (4) is used in OpenLEM to model fluvial erosion and the associated change of topography. Before further discussing the equation variables and the implications of this equation for rivers in steady-state and transient conditions, the next section will briefly discuss the physical mechanisms driving river incision.

4.2.2. Erosion processes

The above introduced detachment-limited stream-power model for river incision is not process specific, meaning that it does not treat the physics of the individual incision processes that act on exposed bedrock (Whipple et al., 2013). However, there are certain parameter values that are more consistent with a specific incision process, as will be discussed later. Therefore it is good to get an overview of the processes that

may act on exposed bedrock, which are (Whipple et al., 2013): Abrasion, plucking, cavitation, weathering and scouring.

Abrasion is the erosion of the bed by energetic collision between travelling sediment grains, either as bedload (hopping and rolling along the bed) or as suspended load in the water column, and exposed bedrock surfaces (Whipple et al., 2013). Every impact does damage to both, the impacting grain and the rock bed. The erosion rate depends on the number of impacts and scales with the sediment flux and the percentage of the bed where rock is exposed (Whipple et al., 2013). Here the dual role of sediment (tools and cover) comes into effect (Sklar and Dietrich, 2004). A greater flux of sediment in transport will lead to a greater number of collisions (tools effect) but will also lead to more of the bedrock being covered by sediment so that a lesser fraction of these collisions will be with exposed bedrock (cover effect) (Whipple et al., 2013; Sklar and Dietrich, 2004).
Plucking of blocks from the bed and banks is an efficient erosion mechanism and the dominant erosion process wherever rocks are fractured at a scale that makes plucking by hydraulic forces possible (Whipple et al., 2013).
Cavitation, the damage to rock surfaces caused by the violent impulsion of small bubbles and c*orrosion*, a suite of weathering and dissolution processes that can weaken rock fabric, joints, and even remove mass also contribute to river incision, primarily by making the rock surface more prone to abrasion and plucking (Whipple et al., 2013).
Debris flow scour is the fifth process, observed where channels are steep and debris flows fast moving. There the passage of the debris flow sweeps the channel clean of its thin layer of alluvium and colluvium cover (Whipple et al., 2013).

All of these incision mechanisms may be at work at the same time at any given point along a bedrock river, so that their interaction may be as important to the overall rate of incision as is the physics of each process independently (Whipple et al., 2013).

4.3. Rivers in steady-state (the graded river)

Both detachment-limited and transport-limited systems approach a steady-state, the graded river. It was Gilbert (1877) application of the principles of energy and thermodynamics to the behaviour of rivers, which lead to the concept of the ‘graded river’, a river in equilibrium, in which the supply of water and sediment are balanced (Grant et al., 2013). Gilbert stated that a river constantly works towards this

equilibrium, primarily by changing its slope (Grant et al., 2013). Mackin (1948) expanded this concept, linking it to Le Chatelier's principle of equilibrium, and extending the ways by which a river can react to a disturbance of the equilibrium state to the full suite of potential channel adjustments (e.g., channel dimensions, grain size) (Grant et al., 2013). Mackin's definition of a graded river is as follows:

> "*A graded stream is one in which, over a period of years, slope is delicately adjusted to provide, with available discharge and the prevailing channel characteristics, just the velocity required for transportation of all of the load supplied from above.*"

This thesis however will use the term steady-state. Steady-state will be defined as in (Whipple et al., 2013), as a condition in which the channel profile has fully adjusted to the climatic, lithological and tectonic conditions upon it. It is important that these factors are invariant over a sufficiently long time to allow the river to adjust its longitudinal profile to the prevailing conditions (Whipple et al., 2013). The time the river takes for this adjustment is termed response time. So steady-state as used in Whipple et al. (2013) refers to a long-term (> ~100 Kyr) condition in which average incision rate balances the average rock uplift rate relative to base-level, so that the longitudinal profile varies only slightly through time. For a detachment-limited channel the steady-state gradient is set by a combination of the river's ability to erode the bed and the prevailing rate of rock uplift or base-level fall (Whipple and Tucker, 2002).

Hack (1957) formulated an empirical relationship between the length of a stream and its drainage area, which laid the groundwork for what is now known as Flint's law (Flint, 1974):

$$S = k_s A^{-\theta} \tag{5}$$

Flint's law states that many steady-state or graded river profiles are well described by a power-law relationship between local channel gradient S and upstream drainage area A, with k_s being the channel steepness index and Θ termed concavity index (Whipple et al., 2013). Hack (1957) recognized that as the shape of the catchment upstream strongly influences the rate at which discharge increases downstream, it consequently influences the rate at which slopes change along a river and therefore the rivers concavity (Kirby and Whipple, 2012). Equation (5) only holds true

downstream of a critical threshold drainage area (A_{cr}) which typically falls in the range of 0.1 – 5 km², as the transition from hillslopes and colluvial channels thought to be dominated by debris-flows to fluvial channels occurs within this range (Kirby and Whipple, 2012). Downstream of this transition, where equation (5) is valid, abrupt spatial or temporal changes in lithology, rock uplift rate, and/or climate may lead to the development of a segmented profile, where each segment shows similar scaling relationship as in equation (5), but with different values of steepness index k_s and concavity index Θ, or both (Wobus et al., 2006).

For a detachment-limited system, if steady-state is defined as a condition in which average incision rate E balances the average rock uplift rate U relative to base-level, then by definition $\partial h/\partial t = 0$ for a channel in steady-state. For such a channel the channel gradient S can be derived by rewriting equation (4) (Howard, 1980; Whipple and Tucker, 2002):

$$S = \left(U/K\right)^{1/n} A^{-m/n} \tag{6}$$

Comparing equations (5) and (6), the following steady-state relationships can be derived (Snyder et al., 2000):

$$\theta = m/n \tag{7}$$

$$k_s = \left(U/K\right)^{1/n} \tag{8}$$

4.3.1. Concavity index Θ and steepness index k_s

Flint's law (Eq. 5) can be rewritten in form of a linear equation by taking the logarithm on both sides of the equation:

$$\log S = -\theta * \log\left(A\right) + \log\left(k_s\right) \tag{9}$$

Given a river follows the scaling relationship of equation (5), plotting the river profile in a log-log plot of slope and area (slope-area plot) should then result in a straight line (Fig. 5). In a segmented river each segment following the scaling relationship should plot as a straight line. The gradient of the line on the slope-area plot is given by Θ, while k_s is given by the intercept of the line with the vertical axis (as can be seen in Eq. 9).

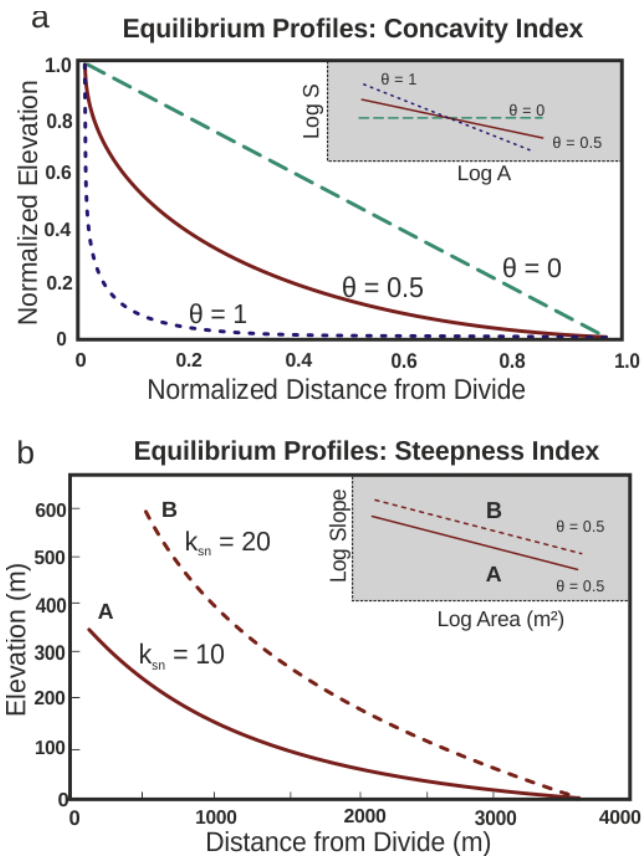

Figure 5: Influence of (a) concavity index Θ and (b) steepness index k_s on steady-state river profiles. (modified after Kirby and Whipple, 2012)

Concavity index *Θ* and steepness index k_s can then be determined by linear regression of this log-log plot of slope and area. Because k_s and *Θ* as determined by regression analysis are strongly correlated and small variations and/or uncertainties in the concavity index lead to wide variations in the steepness index, a reference concavity index Θ_{ref} is required for the interpretation of steepness values (Wobus et al., 2006; Kirby and Whipple, 2012). In practice, Θ_{ref} is usually taken as the regional mean of observed values (Wobus et al., 2006), but because steady-state concavity indices fall into a relatively restricted range, any value of Θ_{ref} between 0.4 and 0.5 should work quite well and a value of 0.45 is often used (Kirby and Whipple, 2012; Lague, 2014). By using a reference concavity index one can determine a normalized steepness index k_{sn} that allows effective comparison of profiles of streams with greatly varying drainage area (Wobus et al., 2006):

$$S = k_{sn} A^{-\theta_{ref}} \tag{10}$$

Determining Θ and k_s by this method relies strongly on digital elevation models (DEMs). DEM data is inherently noisy leading to relatively large scatter in pixel-pixel slope estimates which originates from relatively minor noise in the longitudinal profiles extracted from DEMs (Kirby and Whipple, 2012). By taking the spatial derivative this noise is further exaggerated. There are several procedures to reduce this noise: sub-sampling the long profile, fitting piece-wise linear regressions to the long profile to estimate local slope, applying a moving-average filter to long profile data, and taking log-*A*-bin averages of log *S* (Kirby and Whipple, 2012; Wobus et al., 2006). Alternatively to this procedures one can also measure channel steepness in another way as proposed among others by Perron and Royden (2013) and is referred to as the integral method. Integrating both sides of equation (5) one gets (Kirby and Whipple, 2012):

$$z(x) = k_s \int_{\theta}^{x} A(x')^{-\theta} dx' \equiv k_s \chi(x) \tag{11}$$

This allows determination of the transformed variable $\chi(x)$ (χ, Greek letter chi) directly from drainage area data by numerical integration (Kirby and Whipple, 2012; Harkins et al., 2007). Segments of the channel profile which are well described by a concavity index equal to Θ will be linear on plots of z vs. χ (chi plot; Kirby and Whipple, 2012). The steepness index k_s is then given by the slope of the line. Segments of the channel profile that are not well described by a power-law relation between channel gradient and upstream drainage area, or segments with a concavity index different from the reference value of Θ, will be curved (Kirby and Whipple, 2012).

In simple settings with uniform substrate, uplift rate (and pattern) and climate, the steady-state concavity index Θ falls within a relatively narrow range of ~0.4-0.7 (Kirby and Whipple, 2012; Whipple et al., 2013). It can be influenced by systematic downstream changes in lithology, rock uplift rate, extent of alluvial cover of the bed, and/or runoff (Kirby and Whipple, 2012). Although the concavity index Θ in simple settings falls within a narrow range, one can find concavity indices well outside that range, often related to the river being in a transient state (Whipple, 2004).

In steady-state Θ is insensitive to differences in rock uplift rate, climate or substrate lithology that are uniform along the length of the channel. The steepness index (k_s) on the other hand varies with these factors, which makes it a useful metric for

tectonic geomorphic studies (Kirby and Whipple, 2012; Wobus et al., 2006). The steepness index k_s in general (within a given climate regime and upon substrate of similar strength) is expected to scale in a non-linear way with rock uplift rate *U* and erosion rate *E* (Kirby and Whipple, 2012; Lague, 2014). Lithology can also influence the channel steepness index with harder, less fractured rock being associated with steeper channels, but there are also cases where lithology appears to have no measurable influence (Whipple et al., 2013).

4.4. Rivers in transient state

By defining steady-state as a condition in which the channel profile has fully adjusted to the climatic, lithological and tectonic conditions upon it (Whipple et al., 2013), changing one of these conditions will move the river into a transient state or condition. It is transient because the channels and their surrounding landscape try to reach a new steady-state by adjusting to the new boundary conditions (Whipple et al., 2013). The time a channel needs for this adjustment, the response time, can range from 10^4-10^6 years depending on the erosional efficiency of the channel/hillslope/orogen system, the nature of the perturbation, and the size of the system (Whipple et al., 2013). This thesis will focus on changes in base-level, regionally defined as sea-level, as these will often lead to the formation of migrating knickpoints (Lague, 2014). A change in base-level can be discrete or permanent (Lague, 2014). For the discrete case, a channel is expected to go back the steady-state condition prior to the change, while in the permanent case a new steady-state is attained (Lague, 2014).

4.4.1. Change of base-level

Base-level can be defined by the meaning of the two words base, which means the lowest part, and level, which is a horizontal line or plane positioned along a horizontal axis (Schumm, 1993). Schumm (1993) concludes that therefore base-level is effectively sea-level, although rivers erode slightly below it. This would be the regional definition but base-level can also be defined locally, as a confluence with a higher order stream or by an active tectonic feature (Lague, 2014).

The river response to a change of base-level, defined regionally as sea-level, was among others discussed by Schumm (1993). He made out at least ten variables that are important when regarding the impact of base-level change on the fluvial system. He grouped them into base-level controls (direction, magnitude, rate, and duration),

geological controls (lithology, structure, and nature of valley alluvium) and geomorphic controls (inclination of exposed surfaces, valley morphology, and river morphology and adjustability) (Schumm, 1993).

Regarding *base-level controls*, the direction determines if a river will aggrade or degrade (Schumm, 1993). More important seems the magnitude of base-level change. Small lowering of the base-level can be accommodated by adjustment of the channel slope by changing its pattern or shape, or by increasing bed roughness (Schumm, 1993). A large lowering of base-level will most likely lead to river incision and rejuvenation of the entire drainage network is possible in extreme cases (Schumm, 1993). The rate of base-level lowering plays also an important role. If it is slow a channel can adjust its slope by lateral migration, while when it is fast primarily vertical incision will occur (Schumm, 1993). Rapid incision also leads to a channelization of the flow in a narrow deep channel, which also increases the energy of the flow and further enhances incision (Schumm, 1993). The duration of base-level change is not as important as magnitude and rate but closely related to both (Schumm, 1993).

Geological controls like bedrock or structural controls, can prevent or delay the effect of a base-level change from moving upstream, so that the fluvial system will not be affected until the local control is removed (Schumm, 1993). The valley alluvium determines if incision may propagate upstream. If it is cohesive, incision may be propagate rapidly upstream (Schumm, 1993). A sandy alluvium in a wide and shallow channel can on the other hand dissipate base-level change (Schumm, 1993).

Geomorphic controls are important by means of the surface exposed by base-level lowering, the morphology of the rivers valley and the morphology and adjustability of an alluvial river (Schumm, 1993). Base-level lowering will have a very different impact if it is abrupt, as along a scarp or when lowered gradually, as retreat across a gentle continental slope, which could even be equal to the slope of the river (Schumm, 1993). The valley in which the river flows determines how the river can adjust to the base-level lowering. In a narrow valley a river can only aggrade or degrade, while a channel in a wide valley can also adjust laterally (Schumm, 1993). The influence of the morphology of the river is similar. A river that is straight or sinuous subjected to a steepening of its gradient can become more sinuous and adjust changes of slope without major incision, while a braided river could only incise (Schumm, 1993).

Sea-level lowering to the edge of the continental shelf and down the continental slope will lead to channel incision and the formation of valleys (Schumm, 1993). Large deeply incised valleys will be formed as extension of major rivers draining large areas of the continent, medium-sized valleys as extension of smaller rivers and small valleys will be formed on the shelf by runoff draining from the shelf only (Schumm, 1993).

Schumm (1993) concludes that the effects of base-level change along a large alluvial river probably will be moderate, moving upstream, but not for long distances. Total rejuvenation is therefore not expected but the effect will be greatest where base-level change is great, incision is rapid, and the rivers are confined (Schumm, 1993).

Although Schumm's conclusion mentions alluvial rivers, one should remember that the river morphology can change quickly. Howard et al. (1994) mentioned the dissection of a former alluvial channel system by a sudden drop of base-level as one cause for the occurrence of what they called mixed alluvial-bedrock channels. They state that if base-level is fixed, gradients will gradually diminish up to the point where a minimum gradient, just sufficient to transport sediment supplied from upstream, will be reached. This will convert the affected part of the channel from bedrock to alluvial (Howard et al., 1994). This gradual replacing of the bedrock channel will start at the downstream end and then migrate upstream (Howard et al., 1994). Now, a rapid base-level drop will lead to steepening of the farthest downstream section of the channel and channel slope will be higher than the minimum alluvial channel gradient (Howard et al., 1994). This will reconvert that section into a bedrock-floored knickpoint, which migrates upstream again replacing the alluvial channel section in this process (Howard, 1994). The migration of a knickpoint through a river network in general can lead to modification of multiple channel characteristics such as gradient, width, erosion process, bed morphology, and bed cover characteristics such as grain size and percent bedrock exposure (Whipple et al., 2013).

As the Messinian sea-level fall was fast and with a high magnitude, river response by vertical incision and migration of a knickpoint over great distances is to be expected.

4.4.2. Knickpoints

Howard et al. (1994) defines a knickpoint as a steeper gradient section of channel between lower-gradient sections, as could be produced by a base-level change,

tectonic deformation or change in lithology. Another definition of a knickpoint is given by Whipple et al. (2013). They define a knickpoint as a discrete, mobile boundary between the downstream regions that are adjusted or adjusting to the new forcing and upstream relict regions retaining topographic characteristics of the initial or background forcing.

Gardner (1983) experimentally studied the evolution of a vertical knickpoint after its formation. For his flume experiment he choose cohesive, homogeneous material, as in non-cohesive sediment knickpoints are eroded within geologically short time periods (Gardner, 1983). He describes knickpoint morphology by the terms knickpoint lip, knickpoint face, drawdown reach and intralip angle (Fig. 6a). The *knickpoint lip* is the break in slope where the channel bottom becomes markedly oversteepened. The *knickpoint face* extends from the lip to the base of the knickpoint. The angle between the knickpoint face and the reach above the knickpoint lip is called the *intralip angle*. The *drawdown reach* is that reach of the longitudinal profile where the water surface is oversteepened as a result of drawdown over the knickpoint lip or over the oversteepened reach above the lip (Gardner, 1983). The relation between bottom shear stress τ and critical bottom shear stress needed to initiate motion τ_{cr} along the knickpoint reach governs the morphologic adjustments of an original, vertical knickpoint (Gardner, 1983). Depending on this relationship, Gardner (1983) proposes three models for knickpoint evolution (Fig. 6b): parallel retreat, replacement, and inclination.

Parallel knickpoint retreat needs a resistant caprock or resistant layer (where $\tau_{cr} > \tau$) with an underlying unit of non-resistant material exposed to erosion (where also $\tau_{cr} > \tau$) as well as the removal of material from the plunge pool that forms at the bottom of the retreating knickpoint (Gardner, 1983). These conditions allow for undermining of the caprock and its retreat by collapse and the active formation of a plunge pool (Gardner, 1983). In homogeneous rock knickpoint retreat is possible if pervasive jointing perpendicular to the stream course causing erosional anisotropy exists (Gardner, 1983). Lamb and Dietrich (2009) also reported that vertical waterfalls can persist during retreat due to toppling in well-jointed bedrock (e.g., near horizontal and vertical set of joints as can be found in columnar basalt).
Knickpoint replacement exists in uniformly resistant material where within the knickpoint reach $\tau_{cr} > \tau$ (Gardner, 1983). Erosion of the knickpoint is governed by the

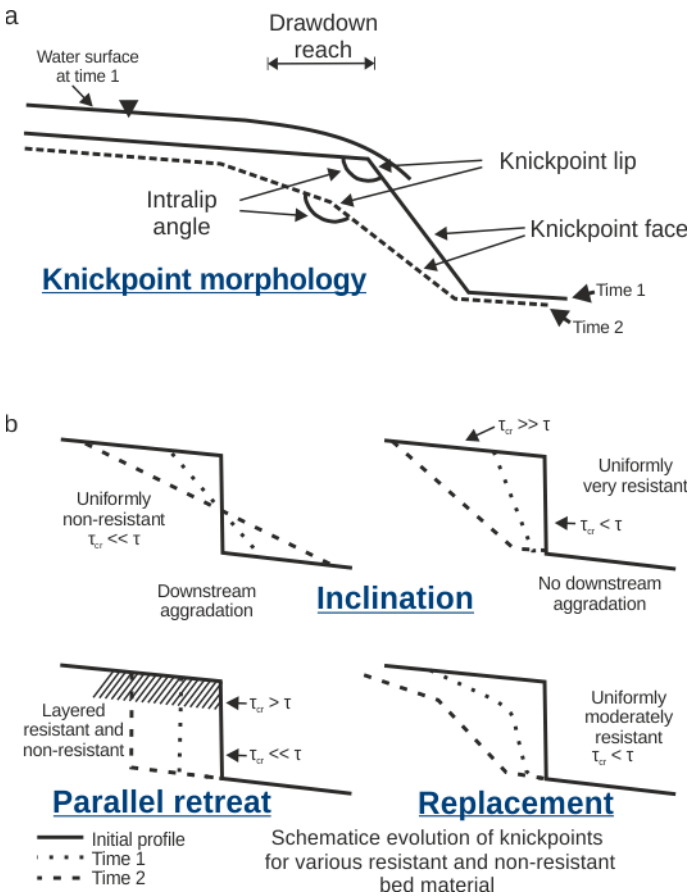

Figure 6: (a) Longitudinal profile of a knickpoint reach. See text for explanation of terminology used to describe knickpoint morphology. (b) Models of knickpoint evolution depending on bed material type and relationship of bottom shear stress τ_0 and critical bottom shear stress needed to initiate motion τ_c. See text for further explanation of the different models. (modified after Gardner, 1983)

behaviour of two components, the reach above the knickpoint lip and the knickpoint face. Replacement of the original vertical knickpoint occurs by decrease of the slope of the knickpoint face while slowly migrating upstream and an increase of the slope of the incised drawdown reach while rapidly migrating upstream (Gardner, 1983). There are two ways of *knickpoint inclination or rotation*, depending on the relation between τ and τ_{cr}. In uniformly non-resistant material, τ_{cr} is frequently less than τ along the knickpoint reach, while in resistant, homogeneous material τ_{cr} is not exceeded upstream from the knickpoint lip (Gardner, 1983). In case of the non-resistant material, this leads to rotation of the knickpoint face with time about some point on the face, as the erosion of the knickpoint face is more rapid than upstream

migration of the drawdown reach (Gardner, 1983). In the case of resistant material, no erosion above the knickpoint lip takes place but τ_{cr} can be exceeded along the knickpoint face. This leads to erosion of the face and the knickpoint rotates about its base (Gardner, 1983).

Gardner (1983) concludes that persistence of a vertical knickpoint while migrating is rare, as they are reduced to a gradual slope by knickpoint replacement and subsequent inclination, and that this elimination of the vertical face occurs early in the evolution of the knickpoint (Gardner, 1983). However parallel knickpoint retreat with persistence of the vertical face is possible under certain conditions, as stated above. A more or less vertical knickpoint face also remains in a fourth model of knickpoint evolution which was added by Frankel et al. (2007). Their experiment used a substrate that was laterally heterogeneous due to vertical interbedding between relative resistant and more easily erodeable layers. The knickpoint evolved close to the replacement model proposed by Gardner (1983) but with the difference that the knickpoint face remained more or less vertical.

4.4.3. Transient channel geometries

Difference in knickpoint evolution leads to different transient channel geometries. Lague (2014) distinguishes three types of transient channel geometries (Fig. 7): Vertical-step knickpoints, slope-break knickpoints and knickzones (Haviv et al., 2010, Whipple et al., 2013).

Vertical-step knickpoints are very steep reaches (rapids) and waterfalls (Lague, 2014). They can have a height from a few to a few hundred meters and can extent from an abrupt vertical waterfall with an undercut plunge pool to a sequence of cascades (Whipple et al., 2013). In a slope-area plot a vertical-step knickpoint will show as a spike (Fig. 7; Whipple et al., 2013).
Slope-break knickpoints are defined by a persistent, longitudinally extensive change in channel gradient, so that they separate channel reaches with roughly identical concavity Θ but different channel steepness k_s values which is easily recognizable in slope-area plots (Fig. 7; Lague, 2014; Whipple et al., 2013). Feedbacks in the river incision process or spatial variation in substrate properties can lead to the formation of vertical-step knickpoints immediately below slope-break knickpoints at the upstream end of the steepened reach (Whipple et al., 2013).
A *knickzone* is a persistent change in downstream channel concavity (Lague, 2014).

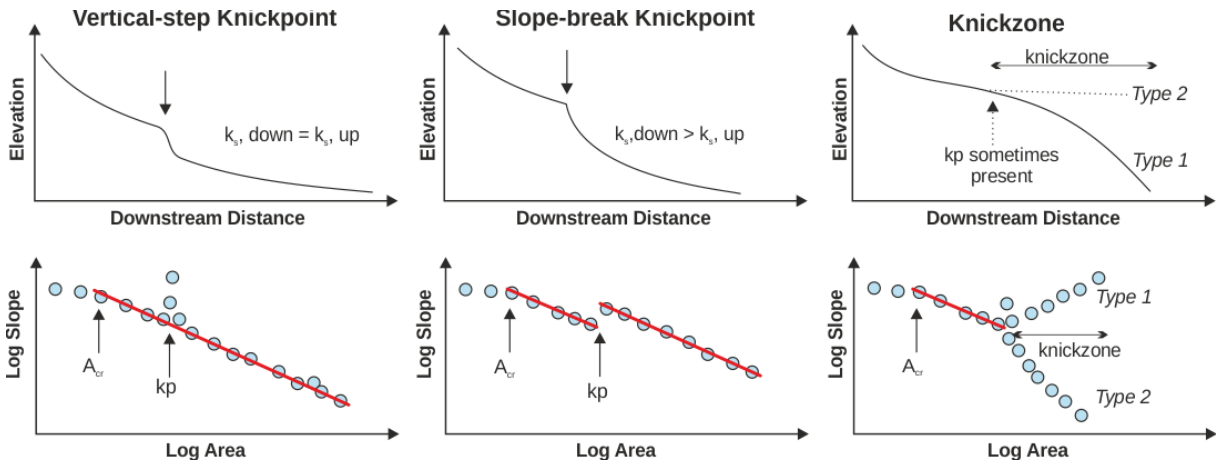

Figure 7: Transient channel geometries and their appearance in longitudinal profiles and slope-are plots. A_{cr} is the critical drainage area below which the slope-area scaling does not hold true. (modified after Lague, 2014)

In contrast to knickpoints, which are local features, knickzones can develop at least over several kilometres to hundreds of kilometres (Lague, 2014).

Mobile vertical-step knickpoints will form in response to discrete, finite drops in relative base-level, as can be caused by sea-level fall, stream capture or a pulse of rock uplift (Whipple et al., 2013). Migration upstream then happens because their local steeper gradient creates greater stresses and potential for incision into bedrock (Whipple et al., 2013). While migrating upstream the knickpoint will lower the base-level at tributary junctions, thereby forming new knickpoints in each tributary (Crosby and Whipple, 2006; Whipple et al., 2013). The retreat rate of vertical-step knickpoints is determined by the water and sediment flux, knickpoint morphology and substrate properties (Whipple et al., 2013).

Mobile slope-break knickpoints in contrast develop in response to a persistent change in boundary conditions like an increase or decrease in the rate of relative base-level fall (commonly set by rock uplift rate) or a change of climate conditions which strengthens or weakens river incision efficiency (Whipple et al., 2013). Where the imbalance between river incision and the rate of relative base-level fall (or rock uplift) is greatest, which is upstream of the knickpoint, most rapid change in relative base-level will take place (Whipple et al., 2013). This imbalance upstream of the knickpoint leads to the upstream migration of the knickpoint (Whipple et al., 2013). Downstream of the knickpoint one can observe both, increase in gradient (and thus incision rate) as well as decrease in gradient (Whipple et al., 2013).

Knickpoints produced by tectonic deformation or base-level change are most likely mobile, migrating upstream and indicative for a river in transient conditions. Knickpoints due to variable rock resistance are often fixed in space and normally do not give information about the condition of the river. Although it is true that mobile knickpoints are a key aspect of all transient landscapes and anchored knickpoints are generally associated with steady-state landscapes, there is no unique correspondence between knickpoint activities and transient landscapes (Whipple et al., 2013). Migrating knickpoints can for instance trigger the formation of hanging tributaries (Wobus et al., 2006), which anchors some knickpoints to tributary junctions for extended periods of time (Whipple et al., 2013).

4.4.4. Transient response in detachment-limited systems

Detachment-limited and transport-limited models can produce equilibrium states that are indistinguishable (Tucker and Whipple, 2002). However they show fundamental differences in their transient behaviour, with an advective nature for a detachment-limited and a diffusive nature for a transport-limited system (Tucker and Whipple, 2002).

The detachment-limited model (Eq. 4) can be rewritten as (Tucker and Whipple, 2002):

$$\frac{\partial h}{\partial t} = -K A^m S^{n-1} \left| \frac{\partial h}{\partial x} \right|, \quad \frac{\partial h}{\partial x} < 0 \tag{12}$$

which can be rearranged for a knickpoint celerity C ($\partial x/\partial t$):

$$C \simeq K A^m S^{n-1} \tag{13}$$

Solutions of equation (12) will take the form of travelling waves (Fig. 8; Tucker and Whipple, 2002). A fundamental implication of equation (12) is that the presence and nature of non-linearity in *n* have a fundamental impact on the shape of stream profiles during transient response (Tucker and Whipple, 2002).

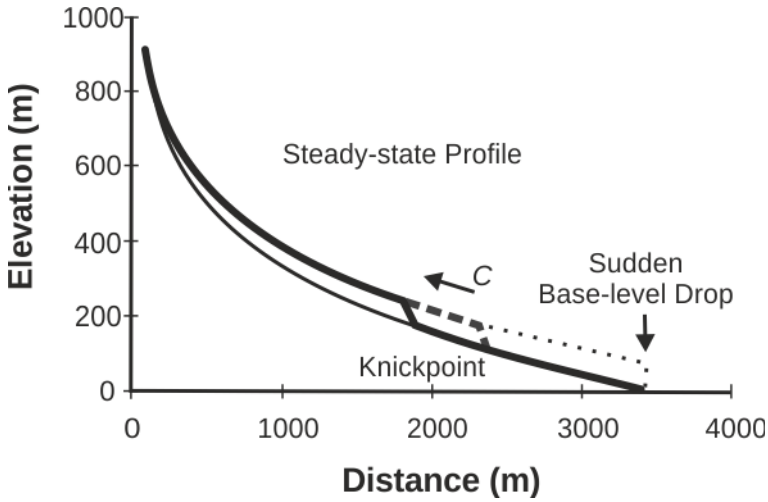

Figure 8: Illustration of a knickpoint migration in response to a sudden base-level fall with C being the knickpoint celerity. (modified after Whipple and Tucker, 2002)

4.4.5. Area exponent *m*, slope exponent *n* and erosion coefficient *K*

This section will focus on the model parameters of the detachment-limited incision model (Eq. 4). It is important to separate model parameters from morphological indices (steepness k_s, concavity θ) (Whipple, 2004). Only under the conditions of steady-state and that both uplift rate U and coefficient of erosion K are uniform through the channel reach equations (7) and (8) hold true (Snyder et al., 2000). Then and only then the parameters $(U/K)^{1/n}$ and m/n can be estimated directly through regressions of channel-gradient and drainage-area data (Snyder et al., 2000).

Regarding knickpoint migration, the value of n plays a fundamental role. For $n = 1$, a detachment-limited stream-power incision model (SPIM) has the form of an advection equation which predicts parallel knickpoint retreat with no dependency on slope S (Eq. 12 and 13; Lague, 2014; Tucker and Whipple, 2002). A vertical-step knickpoint then is the transient response to an instantaneous base-level fall, while an increase in base-level fall rate leads to the formation of a slope-break knickpoint (Lague, 2014; Whipple et al., 2013). When $n \neq 1$ the knickpoint celerity C becomes dependent on the slope leading to the alteration of the knickpoint geometry during propagation (Eq. 13; Lague, 2014; Tucker and Whipple, 2002). For $n > 1$, wave celerity is greater on steeper slopes, and a knickpoint will become a concave-up knickzone with a steep upstream boundary mimicking a slope-break knickpoint (Lague, 2014; Tucker and Whipple, 2002). For $n < 1$, wave celerity is greater on gentler slopes and the knickpoint will progressively become a convex-up knickzone migrating upstream with

a sharp downstream boundary (Lague, 2014; Tucker and Whipple, 2002). Although geometrically similar to field evidence, a SPIM with $n < 1$ cannot match the diffusive nature of transient knickzones documented in different settings (Lague, 2014; Valla et al., 2010). Therefore a more universal alternative to the SPIM is probably needed which combines the behaviour of both detachment-limited (advection) and transport-limited (diffusion) systems to capture for the diversity of transient geometries (Lague, 2014; Whipple and Tucker, 2002). Lague (2014) concludes that while an empirical SPIM with $n = 1$ and $m = 0.5$ fits observations for the migration of knickpoints for many documented cases, it cannot predict the formation of knickzones for any value of m and n. Also the scaling of slope with erosion rate requires for most cases $n \sim 2$ and $m \sim 1$ (Lague, 2014). So that from an empirical perspective, a single set of exponents m and n cannot account for the variety of channel response observed in nature (Lague, 2014). However, the above mentioned inconsistency can be at least partly reconciled by correctly accounting for threshold and discharge variability, effects missing in the original constant discharge derivation (Lague, 2014; Whipple and Tucker, 1999).

Although n and m seem to vary within a wide range, theoretically they are not free parameters but should take on specific values depending on the dominant river incision process (Whipple et al., 2013; Whipple et al., 2000). If plucking is the dominant erosion process then n should be near unity (2/3 to 1), while abrasion by suspended load ($n \sim 5/3$) and cavitation (n as high as 7/3) lead to more non-linear erosion (Whipple et al., 2000). Further if bedrock incision is modelled to be proportional to shear stress rather than stream-power, values of $n \sim 0.7$ and $m \sim 0.3$ are to be expected (Bishop et al., 2005; Howard et al., 1994). Long-term effective values of $n > 2$ can also be related to two effects (erosion threshold and discharge variability) not explicitly considered in a simple SPIM (Lague, 2014; Royden and Perron, 2013). Harel et al. (2016) in their global analysis of the stream power law parameters estimate a value of 2.43 ± 0.15 for the slope exponent n.

The erosion coefficient K is a dimensional coefficient with units of meters^{1-2m} yr^{-1} (Snyder et al., 2000). K is influenced by a wide variety of factors, like channel width and bed material, rock strength, climate, runoff and sometimes includes a threshold term and the influence of the tools and cover effect of sediment (Snyder et al., 2000). Within an area of relatively uniform lithology, K (or analogous erodibility parameter) is

often modelled as constant in both space and time, implicitly assuming that channel gradient is the only variable that is free to adjust to changes in rock-uplift rate (Snyder et al., 2000). However, the factors influencing *K* are thought to adjust during the evolution of a mountain range, as for instance the mentioned decrease in channel width with increase in erosion or uplift rate or increased orographic precipitation due to a higher topography (Snyder et al., 2000). The erosion coefficient is not well constrained, Stock and Montgomery (1999) reporting values of 10^{-2}-10^{-7} $m^{0.2}$ y^{-1}. Harel et al. (2016) estimate an average value of K_{ref} (using m/n_{ref} = 0.5) of $1.2*10^{14}$ ± $3.9*10^{14}$ ($[T^{-1}L^{1-2m}]$), with a median of $2.9*10^{-10}$ ± $1.0*10^{-9}$. They also point out that out of all stream-power law parameters *K* is the most difficult one to estimate.

5. Modelling the evolution of the Messinian Nile canyon

5.1. Study area

This thesis is concerned with the evolution of the Messinian Nile canyon. The area of interest is the Egyptian region, as the canyon cut by the Eonile river extended as far inland as Aswan (Barber, 1981; Said, 1981). For simplification modern day topography was used as a starting point for the modelling, based on the following two assumptions: (1) The course of the modern Nile river in the Egyptian region is closely related with the Messinian canyon (Said, 1981); (2) The structure of northern Egypt evolved during Oligocene and Miocene times and has remained almost inactive since then (Said, 1981).

The actual modelled region extents beyond the Egyptian border to represent a possible Messinian drainage area (Fig. 9). The Messinian drainage area proposed by Griffin (2002) was used as a reference, partly modified by the assumption that the Nile river system connected with the Ethiopian Highlands only in Pleistocene times (Fig. 2; Roden et al., 2011; Said, 1981). Although this also assumes that the Atbara river, as well as the Blue and White Nile rivers, linked with the Nile system only in Pleistocene times, the Atbara river and therefore parts of the Ethiopian highlands are part of the modelled setting. There is no claim that this represents the actual hydrological situation in Messinian times. This thesis also assumes, that capturing of the Qena system by the pre-Nile, as a consequence of the sea-level lowering as proposed by Goudie (2005), happened quite early in the evolution of the Messinian Nile. For simplification, this connection of the two river systems to the Eonile river system was assumed to have already been established at the start of any model run. The resulting drainage area is approximately 1,700,000 km². Due to the modifications made this is less than the 2,100,000 km² as proposed by Griffin (2002) (Fig. 2).

The Eonile river cut its canyon through likely horizontally bedded Eocene and Mesozoic carbonates (Said, 1981; Barber, 1981). In the delta area these Eocene and Cretaceous rocks were topped by likely horizontally disposed Oligocene sands and basalt sheets (Said, 1981). However, for simplification spatial variations in lithology were not regarded for the modelling and a uniform lithology was assumed.

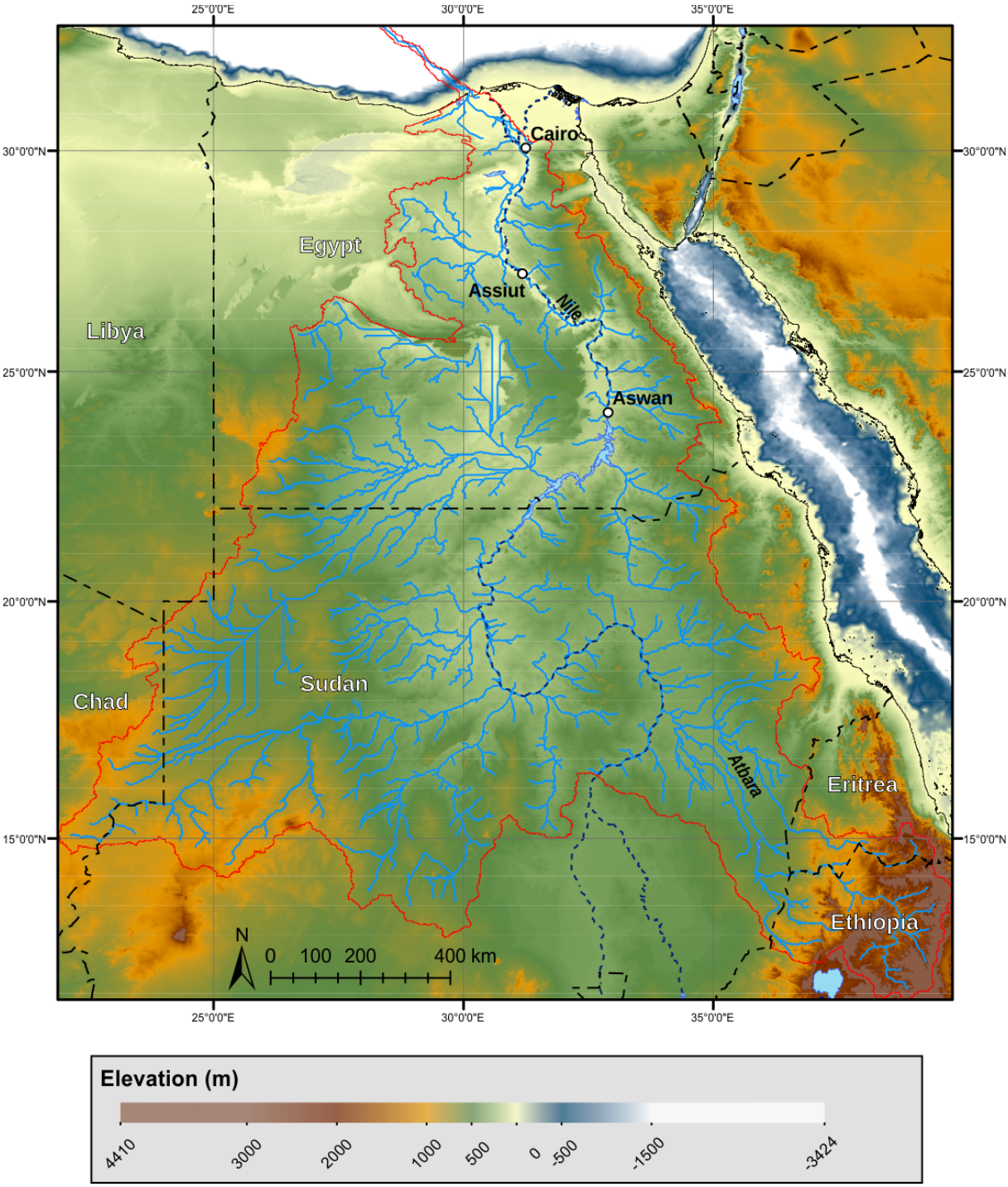

Figure 9: The map shows the modelled drainage area (outlined in red) with the modern river network within that area (solid blue lines) as extracted with the ESRI ArcGIS Hydrology tool. Course of the modern Nile river (dotted blue line), lakes (e.g. Nasser, upstream of Aswan), present day coastlines (thin solid black lines) and political boundaries (dashed black lines) are taken from the GSHHG database (Global Self-consistent, Hierarchical, High-resolution Geography Database; http://www.soest.hawaii.edu/wessel/gshhg/). The map was created using the ESRI ArcGIS software.

5.2. Data and methods

To represent modern day topography SRTM3 (resolution of 3 arc seconds, 90 m at the equator) data for the onshore region was combined with ETOPO1 (resolution of 1 arc minute, 1852 m at the equator) data for the offshore region. Both digital elevation models were projected to a cylindrical equal-area projection and the ETOPO1 data was resampled to a resolution of 90 m. Where in the region of interest there was no SRTM3 data, as for the ocean floor, the ETOPO1 data was then used to fill these gaps. The combined digital elevation model (DEM) was then resampled to a resolution of 1 km, the resolution used for the modelling. All these steps were done using the ESRI ArcGIS software. This DEM consisting of 2451 rows and 2061 columns of 1 km² cells was then loaded into the landscape evolution model (LEM) for further processing. River profile analysis of the results was done with the Stream Profiler tool extension (http://geomorphtools.geology.isu.edu/Tools/StPro/StPro.htm) for ArcGIS, developed by Dr. Benjamin Crosby (Idaho State University).

5.3. Landscape Evolution Model: OpenLEM

OpenLEM is a landscape evolution model developed by Dr. Stefan Hergarten (University of Freiburg). For modelling the evolution of the Messinian Nile only the fluvial erosion module of the software was used, although it does allow for other processes to be modelled (e.g. diffusive erosion, flexural isostasy and landslides). Routing of the water is done by a D8 flow-routing algorithm. The D8 method routes the flow from each pixel toward one of its eight nearest and second nearest neighbouring pixel, depending on the steepest descent (Pelletier, 2013). The software distinguishes between surface elevation and water-level, which allows the filling of depressions as lakes to guarantee a continuous flow network.
OpenLEM implements fluvial erosion by the stream-power erosion model in the form of a detachment-limited erosion model:

$$\frac{\partial h}{\partial t} = U - E = U - K\left(A^{\Theta} S\right)^{n} \tag{14}$$

This equation has the form of equation (4) and implies that the relation $\theta = m/n$ applies (Eq. 7). Uplift rate U, erosion coefficient K, slope exponent n and concavity index θ (and therefore m if $\theta = m/n$ is assumed) are the model parameters. For a

linear stream-power erosion model (n = 1) the new surface elevation and water-level within a cell are calculated implicitly, while for a non-linear model (n ≠ 1) they are calculated explicitly (S. Hergarten, personal communication, 2017).

5.4. Modelling the Messinian river profile evolution

The general idea of this thesis is to examine the influence of the slope exponent n of the detachment-limited erosion model (Eq. 14) on knickpoint geometry. Assuming detachment-limited conditions seems appropriate, as the Messinian Nile actively incised into its bedrock and bedrock rivers tend to be detachment-limited (Whipple and Tucker, 2002; Whipple et al., 2013).

The Messinian sea-level drop initiates a knickpoint of great magnitude which moves upstream through the river network. The slope exponent n greatly influences how this knickpoint evolves in space and time. This has not so much influence on the resulting steady-state river profile but determines the river profile during the transient state. As the Zanclean flooding brought the Messinian incision to an abrupt end before a new steady-state could be obtained, the preserved Messinian canyon represents a river in transient conditions and therefore provides a great example for studying transient river response.

For modelling of the incision of the Messinian Nile river a one-step sea-level fall with a magnitude of 1500 m was assumed. It is thought to have happened in geological instantaneous time. Regarding the duration of the sea-level low-stand no definite constraint was chosen, only that it should lay around 100 Kyr. Models were run till significant incision occurred at Aswan, assuming that this is how far the Messinian Nile cut its canyon.

The Messinian Nile is thought to have cut its channel to a depth of about -1500 m at Cairo (on the basis of reflection seismic data and boreholes; Barber, 1981), about -800 m at Assiut (on the basis of seismic data and loose sediment about 800 m thick overlaying bedrock in Wadi Assiuti; Said, 1981) and about 80-200 m at Aswan (on the basis of observations made during the Aswan dam building; Chumakov, 1973; Loget and Van Den Driessche, 2009). The modelled Messinian river profiles were tested against these three points along the profile to assess their plausibility.

First OpenLEM was used to derive the catchment of the Nile river, which reduced the data to 2169 rows and 1993 columns of 1 km² cells. The main river of this catchment

follows the combined path of the modern Atbara and Nile rivers. The river profile, chi plot and slope-area plot of this river are shown in Fig. 10. For explanation of the plots and the parameter values used in this and all following river profile analysis see the figure caption. This river shows a segmented river profile, where different segments are separated by knickpoints. The major knickpoint of the most downstream part of the river corresponds to the modern day bathymetry of the continental slope in the Nile delta area. The pronounced knickpoint marked with an X in Fig. 10a lies at Aswan. However it is not the knickpoint associated with the Aswan cataract but an artificial knickpoint due to the Aswan dam. The segment between Aswan and the continental slope of the delta area is most likely near equilibrium as no major knickpoint occurs and this segment plots as a straight line in the chi plot. The concavity index θ lies around 0.54 for this segment, but is not well constrained (Fig. 10c). The k_{sn} value of 26.9 is lower compared to the other segments which is due to the very gentle slope of the Nile river in this part of its course. The three river segments upstream of Aswan also show $\theta \sim 0.5$, with two of them being well constrained. The k_{sn} values for these three segments lie between 70 and 130. The knickpoints separating these three segments also show in the chi plot (Fig. 10b), meaning that they are mobile, as stationary knickpoints associated with, for example, changes in bedrock erodibility or precipitation, disappear in a dimensionless profile (Royden and Perron, 2013). The nature of these knickpoints and more thoroughly analysis of the modern river profile are not part of this thesis.

Next OpenLEM was used to produce an equilibrium topography of this catchment, using a linear stream power erosion model (n = 1), a concavity index of $\theta = 0.5$ and an uplift rate U = 75 m Myr^{-1} (Fig. 15 and 16). The chosen uplift rate is fictional, producing an equilibrium river profile which is close to the modern day river profile in the most downstream parts of the Nile river (Fig. 15a). Again, the uplift rate as well as the equilibrium river profile, are not thought to represent the actual situation prior to the Messinian Crisis. Equilibration of the river profile was rather done to remove any influence of modern topography on the evolution of the knickpoint. Equilibration of the main rivers tributaries was not finished as can be seen by the wider range of k_{sn} values within these tributaries compared to the quite consistent values within the main river (Fig. 15c).

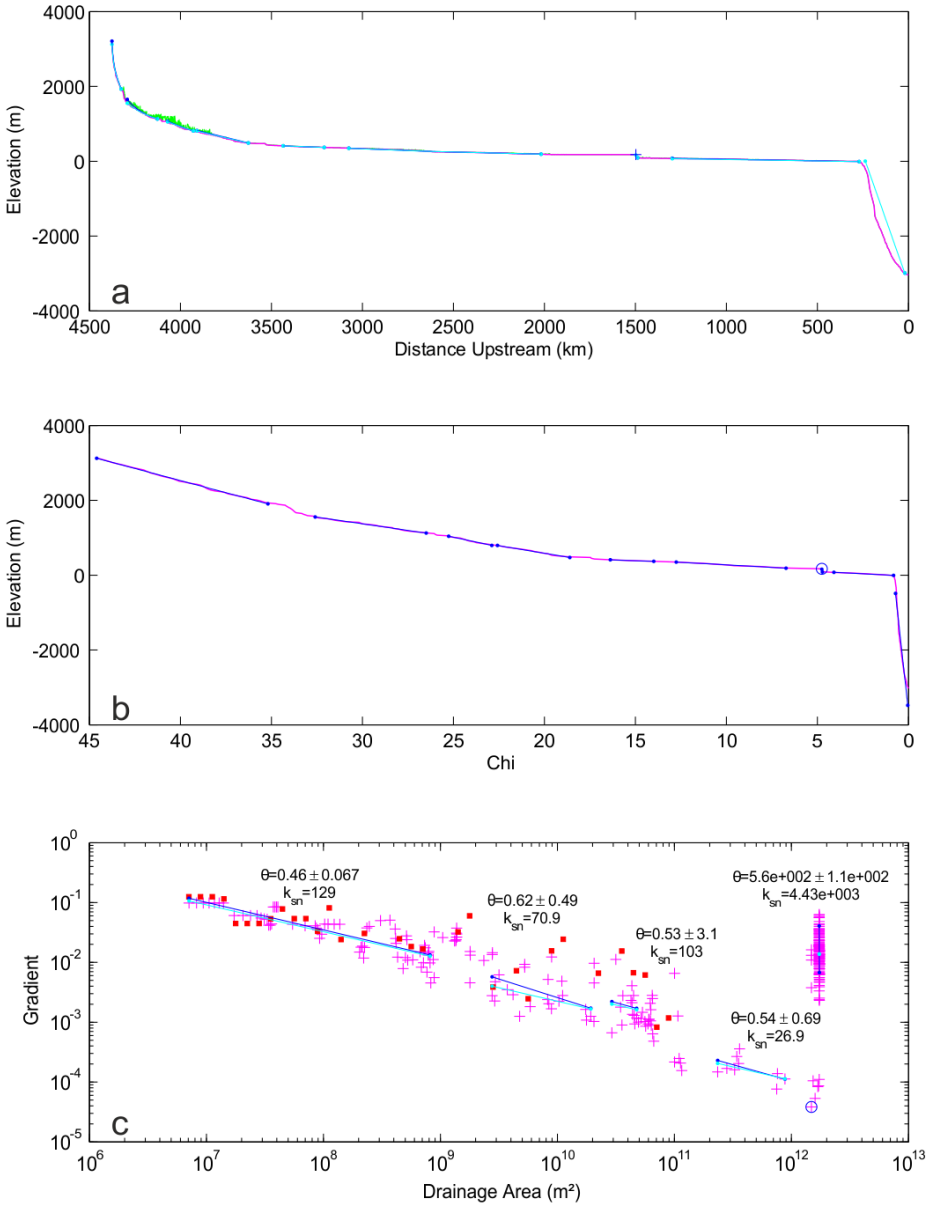

Figure 10: River profile analysis for the combined Atbara and Nile rivers. Analysis was done using Θ_{ref} = 0.45, smoothing window of 3 km (three times cell size), sampling interval of 20 m, and auto k_{sn} window of 3 km. (a) Longitudinal river profile, segmented by knickpoints. The artificial knickpoint associated with the Aswan dam is marked by a X. (b) Chi plot for the river profile, with segments separated by knickpoints, as associated with rivers in transient condition. A river in steady-state should plot as a straight line. The Aswan dam knickpoint is marked by a circle. (c) Slope-area plot for segmented river. For a river in steady-state all points should lie within a line. Concavity index Θ and normalized steepness index k_{sn} as determined by regression are shown. The point associated with the Aswan dam knickpoint is again marked by a circle. For all three plots, the dark blue line shows profiles (or lines) predicted by the regressed channel concavity Θ, while the cyan lines show the profiles (or lines) for the specified reference concavity Θ_{ref}. In the lower plot red squares are log-bin averages of the slope-area data. Plots were created using the Stream Profiler tool, developed by Dr. Benjamin Crosby (Idaho State University).

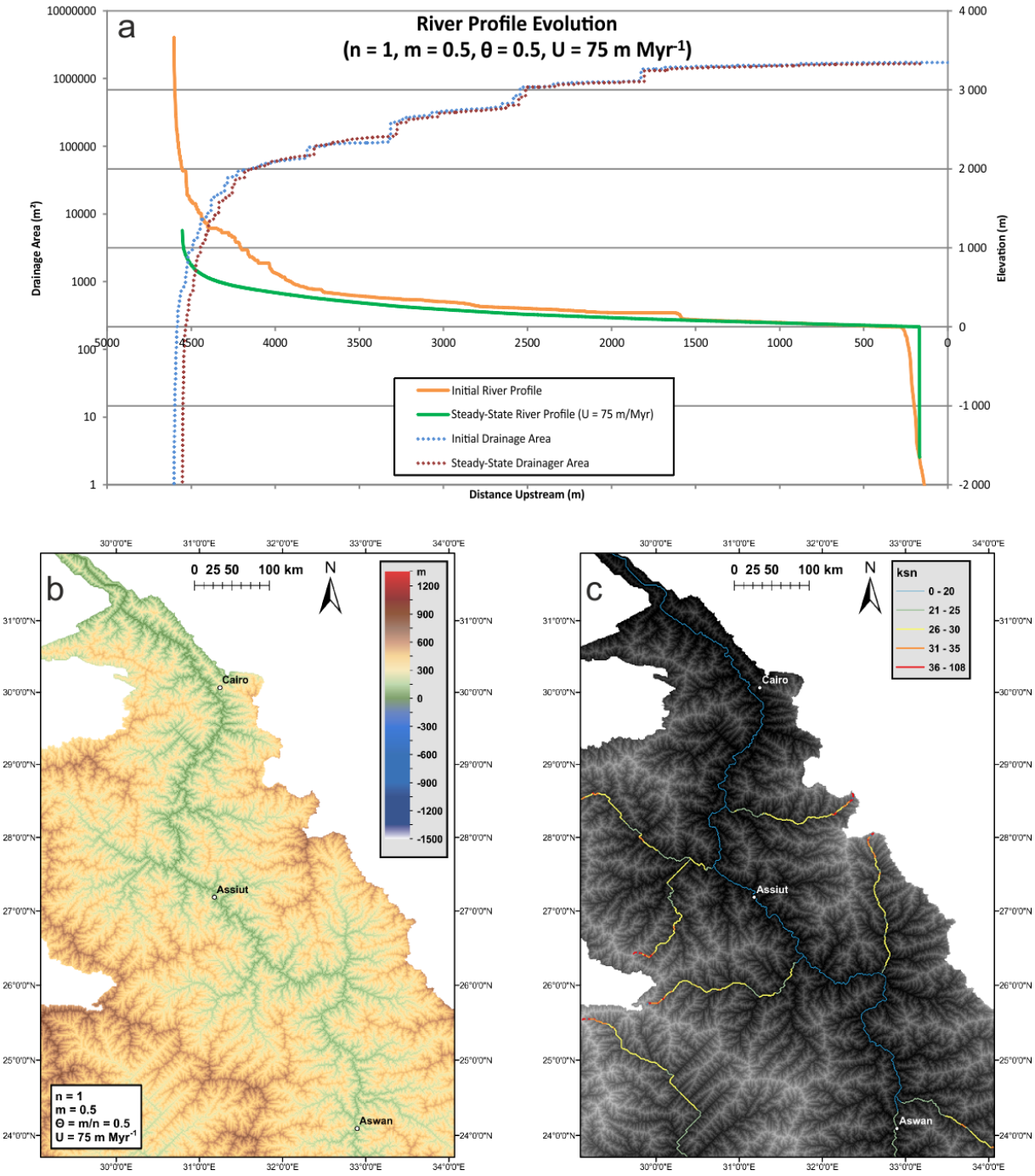

Figure 11: (a) River longitudinal profiles of the initial river profile (orange) and the steady-state (equilibrated) river profile (green) with corresponding drainage area. (b) Topographic map of the model region up to Aswan, after equilibration of the initial topography (corresponding to green river profile). (c) Map of k_{sn} values for the equilibrated topography on top of grey-scale topography. Model parameters for the equilibration of the initial topography can be seen in (a) and (b). Maps were created using the ESRI ArcGIS software and Stream Profiler tool extension (as developed by Dr. Benjamin Crosby of the Idaho State University).

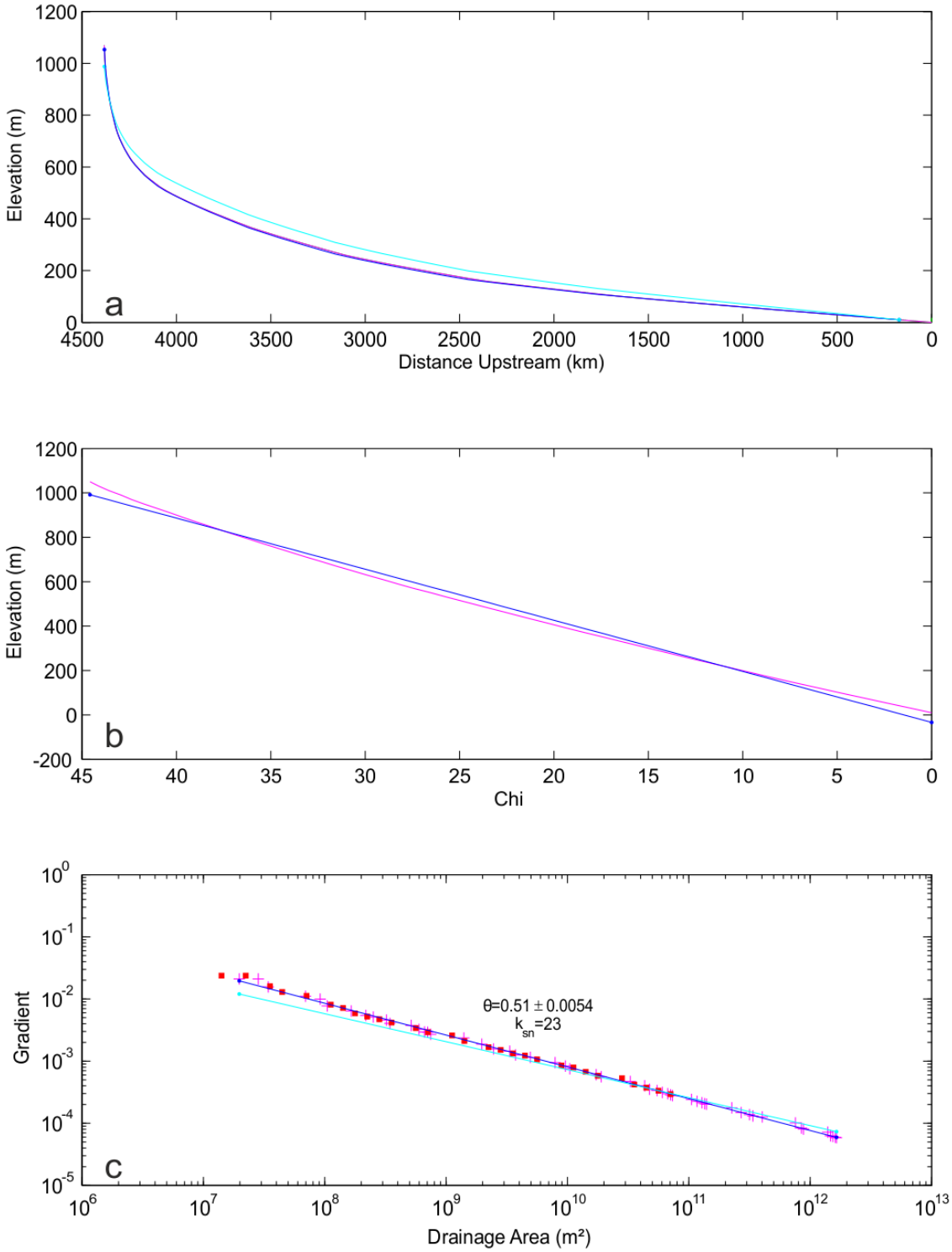

Figure 12: River profile analysis for the equilibrated Nile river. (a) Longitudinal river profile, showing the characteristic logarithmic river profile for a river in steady-state. (b) Chi plot for the equilibrated river profile. A river in steady-state should plot as a straight line. (c) Slope-area plot for the equilibrated river. For a river in steady-state all points should lie within a line. Concavity index Θ and normalized steepness index k_{sn} as determined by regression are shown. For parameters used and further explanation (blue and cyan lines etc.) see Fig. 10.

This equilibrated DEM was used as starting point for any model run. The drainage area for this Messinian Nile river is 1,649,450 km². To simulate the Messinian sea-level drop the water-level in the most downstream cell of the drainage network was set to -1500 m. This initiates the knickpoint which then starts moving upstream the drainage network in the successive erosive steps. The three points used to evaluate the modelled river profile lie ~345 km (Cairo), ~790 km (Assiut) and ~1385 km (Aswan) upstream of the rivers mouth.

Each model run was done using a time step of $dt = 10^{-5}$ Myr = 10 yr. Model output was saved after every 100 iterations (1000 yr) of erosion. For simplification K was kept constant in space and time throughout each model run, assuming uniform rock strength and climate. No uplift ($U = 0$ m Myr^{-1}) occurs during the model runs. As K and U are thus uniform in the modelled region, the relationship $\theta = m/n$ (Eq. 7) holds true. Apart from the fluvial erosion model component, none of the other model components (diffusive erosion, flexural isostasy, landslides etc.) were active during the model runs. This was done to keep the modelling simple and isolate the effect of the detachment-limited erosion model. Neglecting hillslope processes may be valid as incision and subsequent filling of the Nile canyon may have been too fast for hillslopes to respond significantly (Loget et al., 2006). However, isostatic response of the continental margin to the desiccation of the Mediterranean and the related deposition of evaporites is to be expected (Govers et al., 2009; Gargani et al., 2010) but was not regarded in the model runs.

This thesis does not try to quantify knickpoint migration rates as they are highly dependent on the erosion coefficient K. As K is only roughly constrained and influenced by various factors, estimations for its actual value for the Messinian Nile are difficult to make. Of course assuming the duration of the erosional phase and knowing how far inland (as far as Aswan) the Messinian Nile cut its channel, one can constrain the K value to a certain extent. This was done and will be discussed in more detail at the appropriate place.

The main interest lies in the alteration of the knickpoint geometry in time and the resulting transient river profile but not so much in the actual absolute time within these profiles. Seven different model runs were executed (results are shown for model runs one to six), with the focus on the effect of different values for the slope-exponent n on the transient evolution of the river profile. Table 1 shows the full set of

model parameters used in the individual runs, as well as the amount of incision at Cairo, Assiut and Aswan at the end of each of the model runs.

Model run	*n*	*Θ*	*m*	*K* [m^{1-2m} yr^{-1}]	K [m^{1-2m} Myr^{-1}]	*dt* [Myr]	time steps	*t* [Kyr]	Incision at time *t* [m]		
									Cairo	Assiut	Aswan
1	1	0.5	0.5	1.00E-005	1.00E+001	1.00E-005	105	105	-1500	-1500	-72
2	0.5	0.4	0.2	1.00E-003	1.00E+003	1.00E-005	85	85	-1500	-698	-360
3	0.75	0.4	0.3	2.50E-004	2.50E+002	1.00E-005	77	77	-1500	-806	-131
4	1.5	0.5	0.75	1.00E-007	1.00E-001	1.00E-005	120	120	-1479	-1252	-154
5	2	0.5	1	1.50E-009	1.50E-003	1.00E-005	150	150	-1419	-1074	-176
6	2.5	0.5	1.25	2.50E-011	2.50E-005	1.00E-005	90	90	-1367	-971	-179
7	2	0.4	0.8	5.00E-008	5.00E-002	1.00E-005	75	75	-1416	-1062	-170

Table 1: Parameters for the individual model runs are shown, as well as the duration of each model run (time t) and the incision at Cairo, Assiut and Aswan at the end of each run.(n: slope exponent; Θ: concavity index; m: area exponent; K: erodibility; dt: time step; t: time)

6. Results

Model run one was done using n = 1, m = 0.5 and θ = 0.5 (linear SPIM; Model run 1 in Tab. 1) as parameters. The evolution of the river profile (Fig. 13a) shows that the knickpoint approximately keeps its steep geometry while moving upstream and moves with a near constant velocity. Upstream of the knickpoint minor erosion and lowering of the river profile occurs, without changing the characteristics (θ and k_{sn}) of the initial (equilibrated) river profile (Fig. 13 and 14). In the k_{sn} map (Fig. 13c) the knickpoint shows as a stretch with high k_{sn} values, and thus high stream-power, just downstream of Aswan. Highest k_{sn} values are associated with the steep knickpoint face. Stretches of high k_{sn} values in the tributaries are due to knickpoints which initiated by the lowering of the local base-level by the migrating knickpoint of the main river. The knickpoint is also readily distinguished in the slope-area plot as a near vertical spike, and also shows in the river profile and chi plot (Fig. 14). The erosion reaches Aswan after approximately 105 Kyr. As the steep initial knickpoint geometry is maintained, the incised canyon reaches a depth of 1500 m for nearly its whole length. This leads to overestimation of incision at Assiut, where only around 800 m of Messinian incision is to be expected.

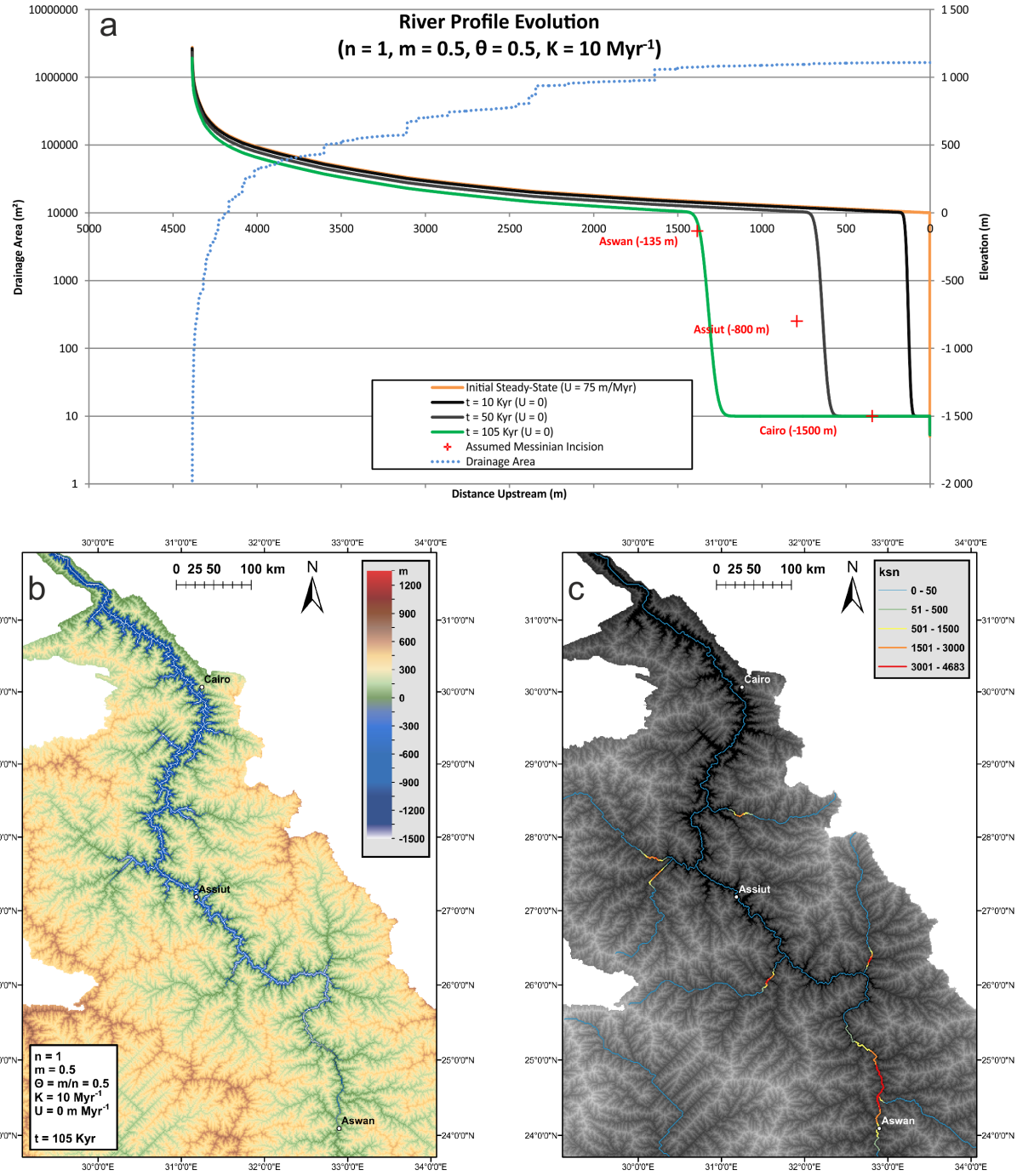

Figure 13: Results for model run one (n = 1). (a) Evolution of the longitudinal river profile in time. Note that the vertical axis is exaggerated. Green river profile represents final state, after which the model run was stopped. Red crosses mark the expected incision depth (in brackets) at the three points Cairo, Assiut and Aswan, against which the modelled river profile is tested. It can be seen that the initial steep knickpoint geometry is kept during the river profile evolution. (b) Topographic map of the model region up to Aswan after the final modelling step, corresponding to the green river profile. (c) Map of k_{sn} values after the final modelling step on top of grey-scaled topography for the model region up to Aswan. High k_{sn} values (and thus stream-power) correspond to the steep knickpoint face. Model parameters for this model run can be seen in (a) and (b).

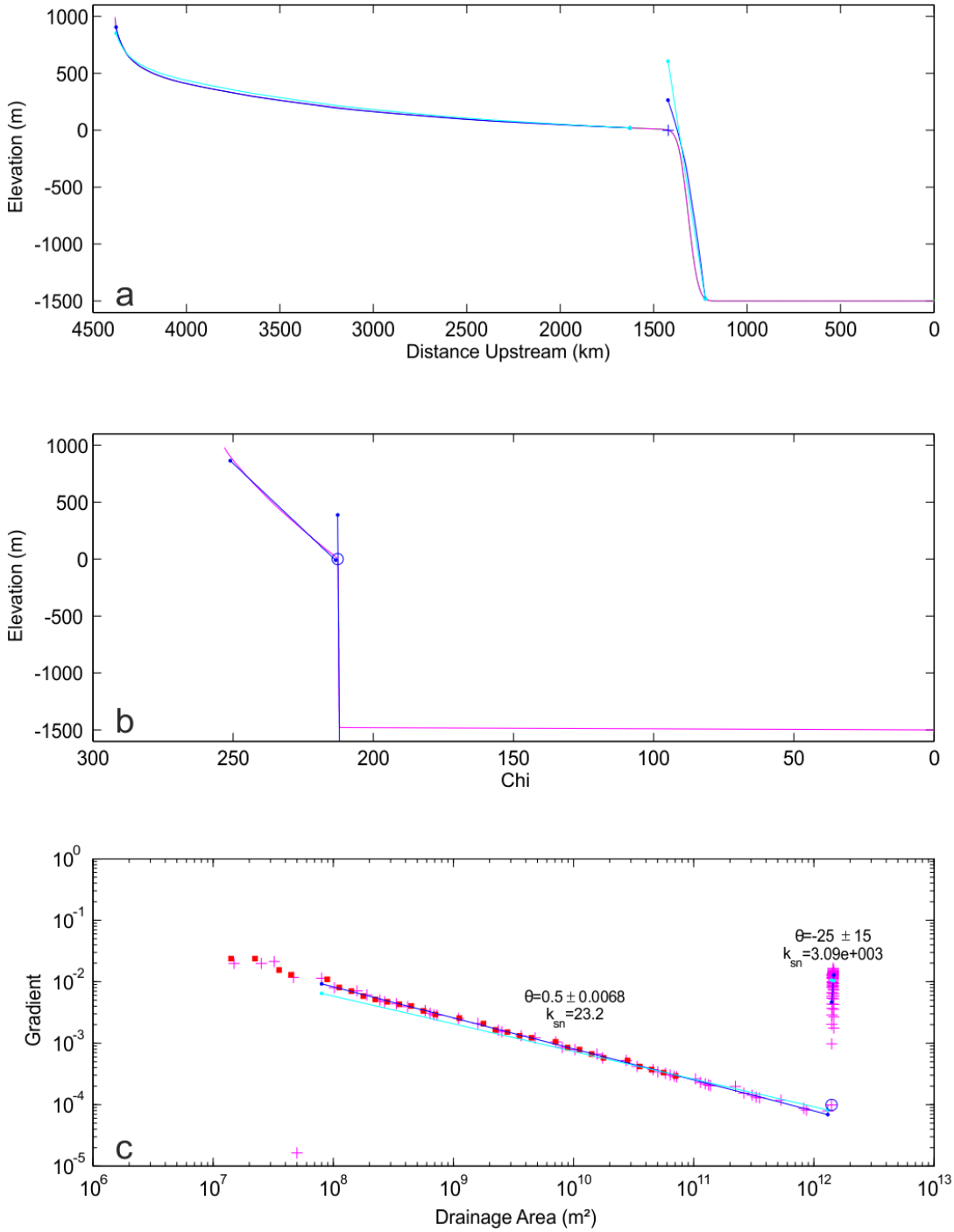

Figure 14: River profile analysis for model run 1 (n = 1). (a) Longitudinal river profile, showing the steep knickpoint. (b) Chi plot showing the segmented river profile, the segments separated by a knickpoint and each segment plotting as an approximately straight line, indicative for a river in steady-state. (c) Slope-area data, where the knickpoint shows as a spike with a high and negative concavity index Θ, and the ancient part of the river upstream the knickpoint showing the characteristics of the equilibrated river profile (Θ = 0.5), prior to sea-level fall. The cross in the longitudinal profile shows location of the knickpoint, corresponding to circles in second and third plot. For parameters used and further explanation (blue and cyan lines etc.) see Fig. 10.

For model runs two (n = 0.5, m = 0.2, θ = 0.4, K = 1000 $m^{0.6}$ Myr^{-1}) and three (n = 0.75, m = 0.3, θ = 0.4, K = 250 $m^{0.4}$ Myr^{-1}) the slope exponent n is lower than unity (Tab. 1). In these cases the knickpoint evolves by keeping a steeper knickpoint face in its lower part while the knickpoint lip changes in a diffusive manner (Fig. 15a and 17a). This is accompanied by significant erosion immediately upstream of the knickpoint lip, steepening of the drawdown reach and increase of the intralip angle. Thus with time the initial sharp knickpoint evolves into a convex-up knickzone. As a whole this knickzone moves upstream and not just rotates about its initial base. A higher value of n results in a steeper and shorter knickzone. Further upstream of the knickpoint lip the whole river profile incises significantly but approximately keeps the characteristics of the initial river profile. For both model runs decay of the topography below modern sea-level and some artefacts at the model boundary are observed (Fig. 15b and 17b). For model run two, the knickzone leads to higher k_{sn} values for the whole stretch between Aswan and Cairo, while for model run three the knickzone only stretches from Aswan to around 150 km south of Assiut (Fig. 15c and 17c). Highest k_{sn} values are found at the most downstream part of the knickzone, where its steepest, with higher absolute values for a higher value of n. Again migration of the knickpoint into the passed tributaries can be observed. The knickzone can be seen in the river profiles and chi plots and is easily distinguished in the slope-area plot as one (Model run three) or two (Model run two) steep spikes with a negative gradient (Fig. 16 and 18). For the used erosion coefficients K, the erosion reaches Aswan after 85 Kyr (Model run two) and 77 Kyr (Model run three) respectively. The second model run with n = 0.5 underestimates incision at Assiut (689 m) while overestimating the incision at Aswan (360 m) (Fig. 15a). The third model run with n = 0.75 produces a river profile which approximately fits the expected Messinian river profile (Fig. 17a). Incision reaches the expected 1500 m at Cairo, 806 m at Assiut and 131 m at Aswan (Table 1).

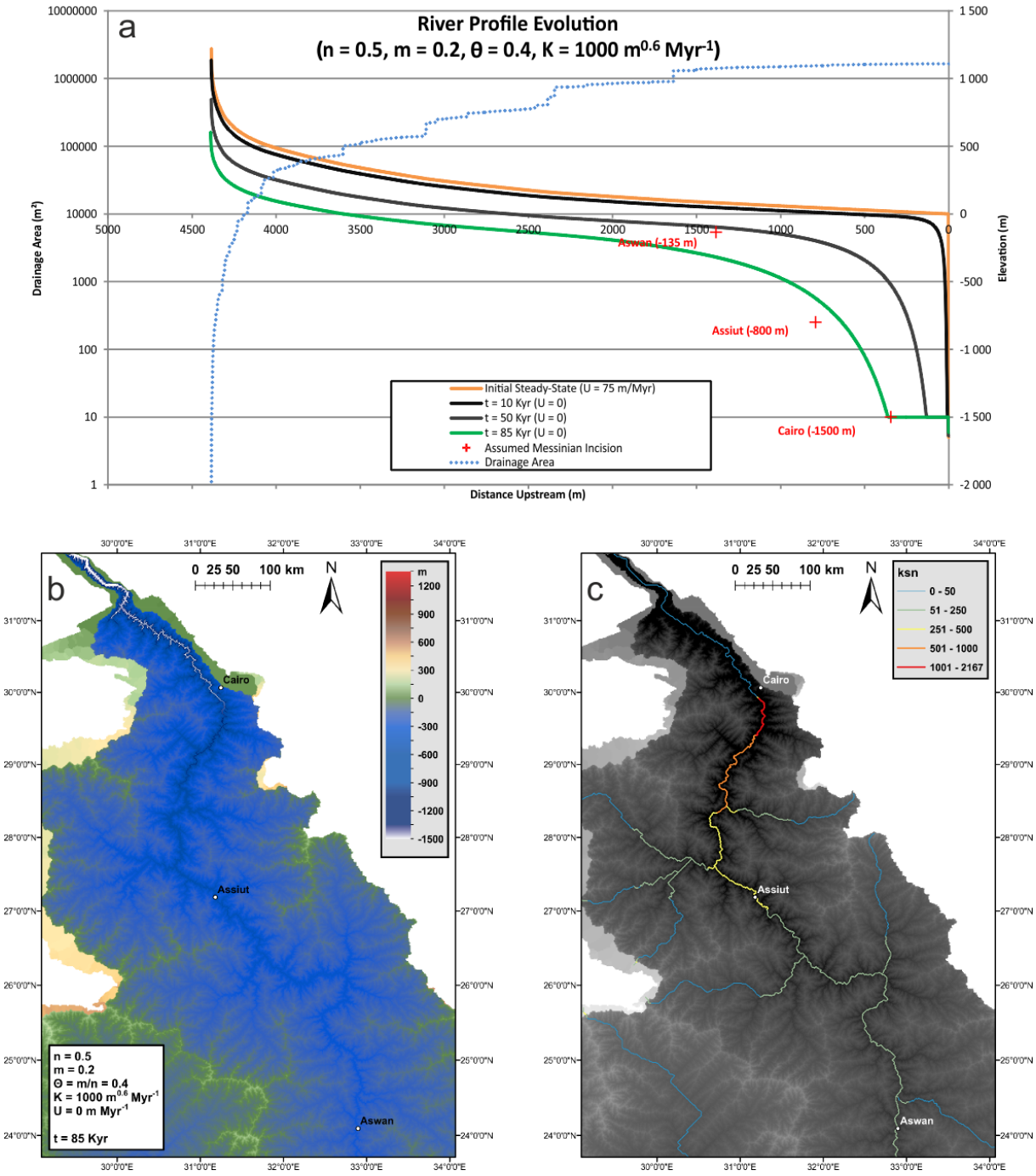

Figure 15: Results for model run two (n = 0.5). (a) The initial steep knickpoint evolves by a diffusive like erosion of the knickpoint lip, while keeping a steeper knickpoint face in its lower part. In time this leads to the formation of a convex-up knickzone. As a whole this knickzone moves upstream. Incision also occurs upstream of the knickpoint lip, leading to steepening of the drawdown reach. (b) Topographic map of the model region up to Aswan after the final modelling step, corresponding to the green river profile. The topography decays below modern sea-level and shows some artifacts at the model boundary. (c) Map of k_{sn} values after the final modelling step. Highest k_{sn} values (and thus stream-power) correspond to the lower, steeper part of the knickzone. For further explanation of the shown river profiles and maps see Fig. 13. Model parameters for this model run can be seen in (a) and (b).

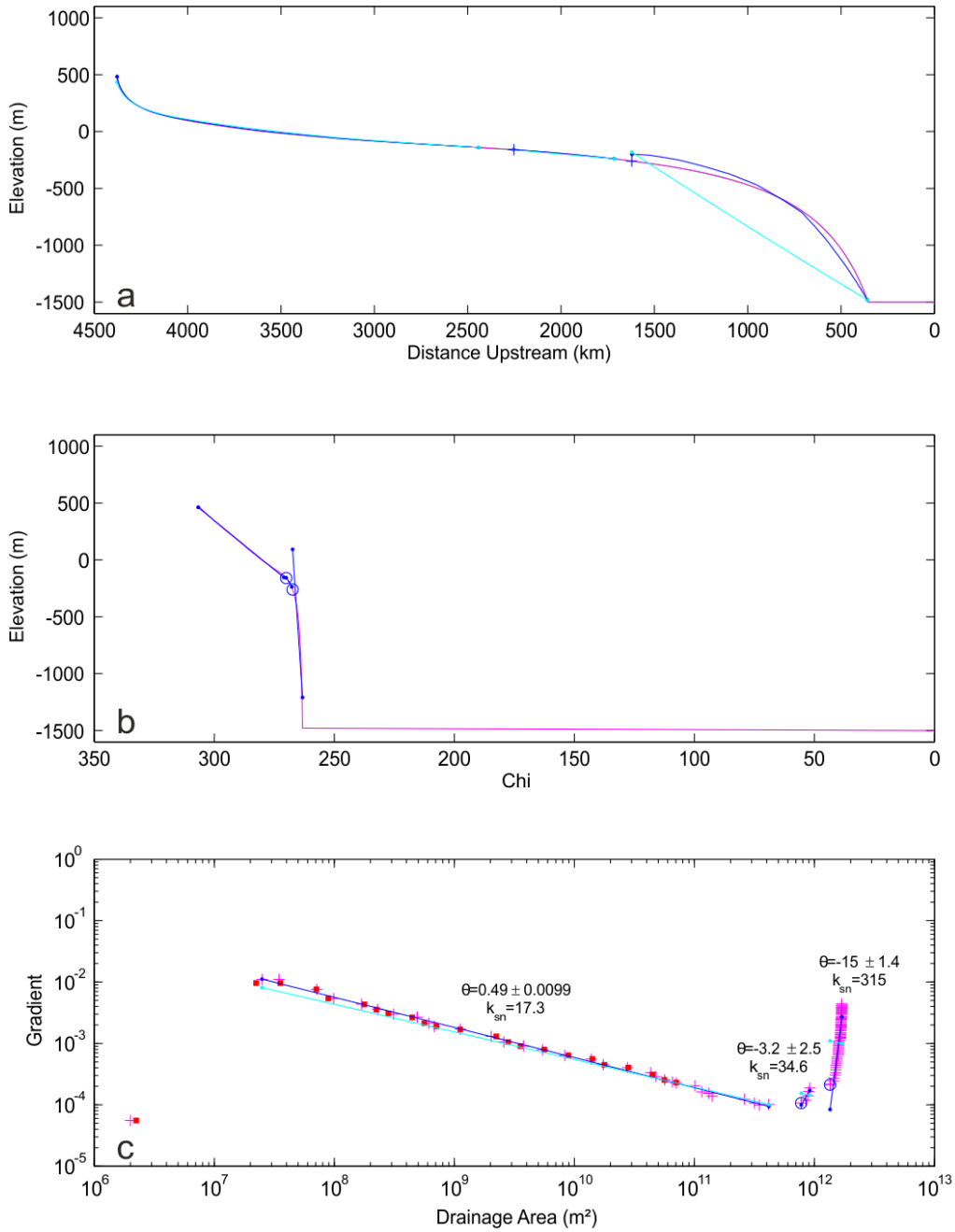

Figure 16: River profile analysis for model run two (n = 0.5). (a) Longitudinal river profile, showing a concave-up knickzone. (b) Chi plot showing the segmented river profile, each segment plotting as an approximately straight line, indicative for a river in steady-state, separated by a very steep part corresponding to the knickzone. (c) Slope-area data, where the knickzone shows as two spikes with high and negative concavity index Θ, the smaller spike corresponding to a steeper drawdown reach upstream of the knickzone and the bigger spike to the knickzone itself. The ancient part of the river upstream of the drawdown reach shows the characteristics of the equilibrated river profile (Θ = 0.5), prior to sea-level fall. The crosses in the longitudinal profile shows location of the beginning of the steeper drawdown reach and beginning of the knickzone, corresponding to circles in second and third plot. For parameters used and further explanation (blue and cyan lines etc.) see Fig. 10.

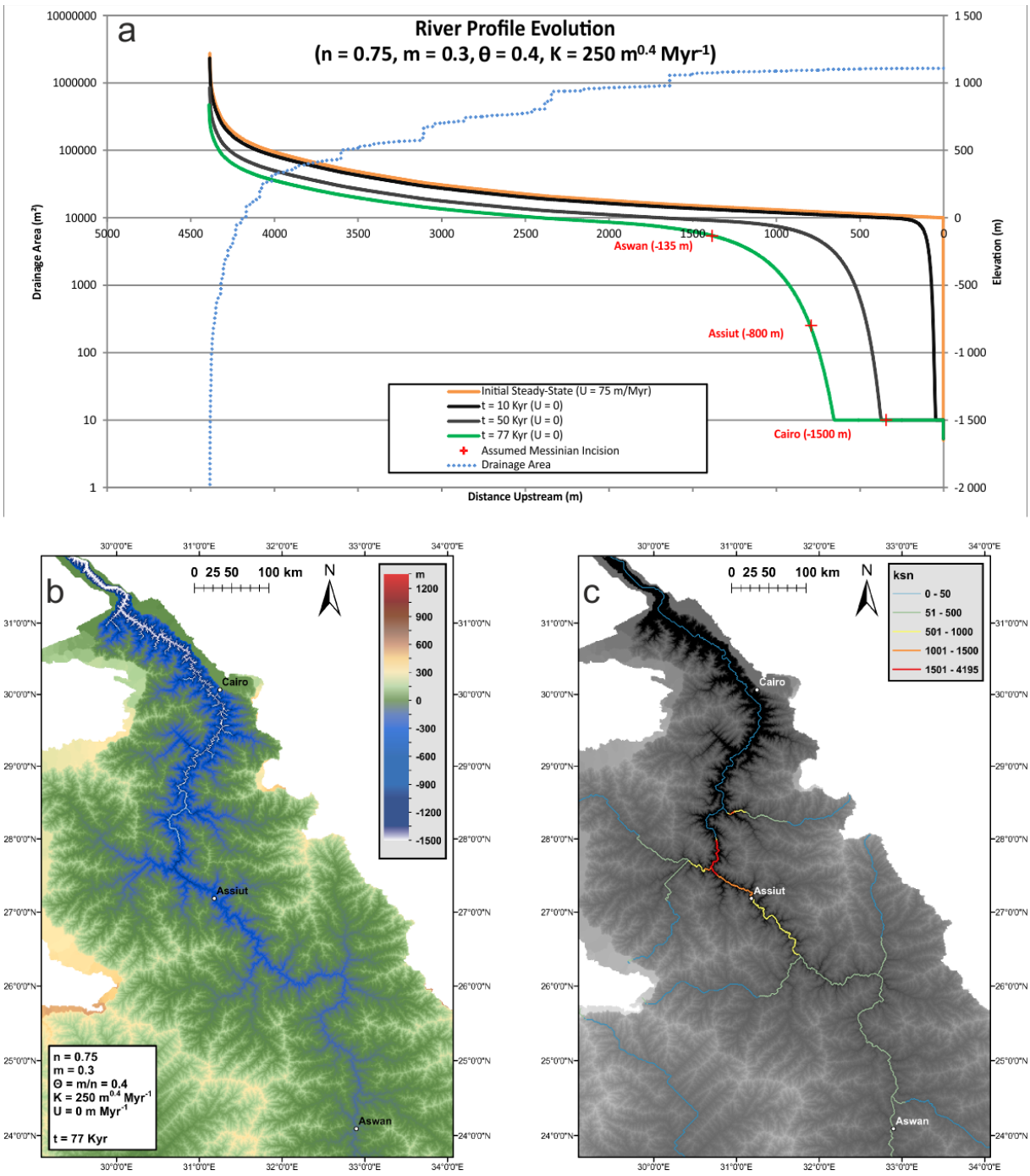

Figure 17: Results for model run three (n = 0.75). (a) The initial steep knickpoint evolves by a diffusive like erosion of the knickpoint lip, while keeping a steeper knickpoint face in its lower part. In time this leads to the formation of a convex-up knickzone. As a whole this knickzone moves upstream. Incision also occurs upstream of the knickpoint lip, leading to steepening of the drawdown reach. (b) Topographic map of the model region up to Aswan after the final modelling step, corresponding to the green river profile. The topography decays below modern sea-level and shows some artifacts at the model boundary. (c) Map of k_{sn} values after the final modelling step. Highest k_{sn} values (and thus stream-power) correspond to the lower, steeper part of the knickzone. For further explanation of the shown river profiles and maps see Fig. 13. Model parameters for this model run can be seen in (a) and (b).

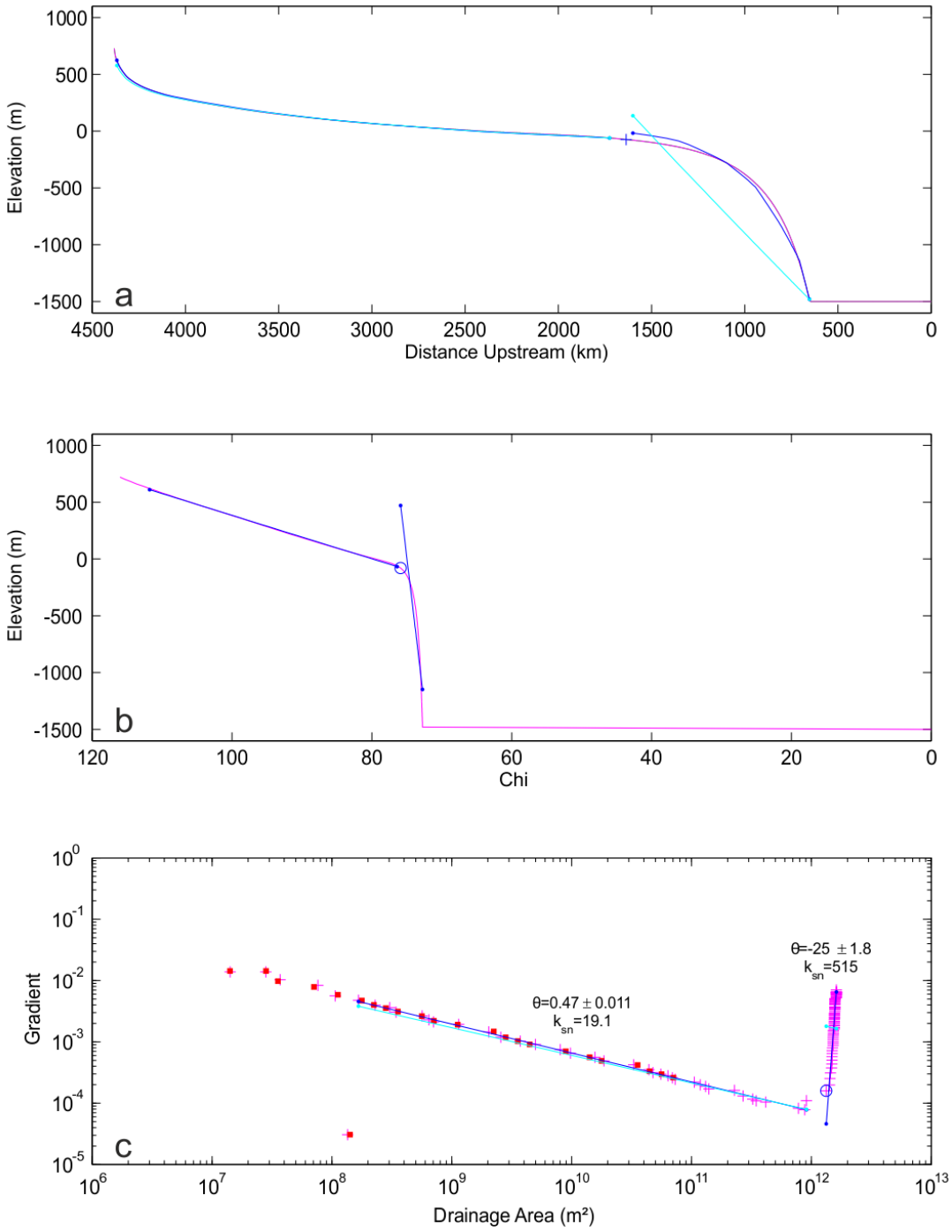

Figure 18: River profile analysis for model run three (n = 0.75). (a) Longitudinal river profile, showing a concave-up knickzone. (b) Chi plot showing the segmented river profile, each segment plotting as an approximately straight line, indicative for a river in steady-state, separated by a very steep part corresponding to the knickzone. (c) Slope-area data, where the knickzone shows as a spike with a high and negative concavity index Θ. The ancient part of the river upstream of the knickzone shows the characteristics of the equilibrated river profile (Θ = 0.5), prior to sea-level fall. The cross in the longitudinal profile shows location of the beginning of the knickzone, corresponding to circles in second and third plot. For parameters used and further explanation (blue and cyan lines etc.) see Fig. 10.

For model runs four (n = 1.5, m = 0.75, θ = 0.5, K = 0.1 $m^{-0.5}$ Myr^{-1}), five (n = 2, m = 1, θ = 0.5, K = 0.0015 m^{-1} Myr^{-1}), six (n = 2.5, m = 1.25, θ = 0.5, K = 0.000025 $m^{-1.25}$ Myr^{-1}), and seven (n = 2, m = 0.8, θ = 0.4, K = 0.05 $m^{-0.6}$ Myr^{-1}) the slope exponent n is greater than unity (Tab. 1). The knickpoint evolves by rotating around its initial point at the base of the knickpoint face, leading to a slope-break knickpoint (Fig. 19a, 21a and 23a). At the knickpoint lip the knickpoint remains sharp throughout these model runs. Upstream of the knickpoint lip nearly no incision occurs and the river retains its initial characteristics. No steepening of the drawdown reach is observed. As a whole the knickpoint does not move upstream significantly but only rotates about its base. Higher k_{sn} values (compared to initial profile) can be observed for the whole part of the river profile from its most downstream point up to Aswan (Fig. 19c, 21c, 23c). Highest values are observed at the most upstream part of the knickpoint, near the knickpoint lip. In general higher k_{sn} values are observed for lower values of slope exponent n. In the slope-area plots the slope-break knickpoint shows as a steep spike with a positive gradient and is also distinguishable in the river profiles and chi plots (Fig. 20, 22 and 24). As the knickpoint only rotates about its base and does not move upstream, a base-level fall of 1500 m underestimates incision at Cairo. For a value of n = 1.5 this underestimation is low (1479 m; Model run four; Fig. 19a) but gets bigger for higher values of n (1367 m for n = 2.5; Model run six; Fig. 23a). At Assiut all these model runs overestimate incision, overestimation being higher for lower values of n. At Aswan all these model runs incise between 154 m (n = 1.5; Model run four) and 179 m (n = 2.5; Model run six), all within the reach of expected Messinian incision. The best fit river profile for n > 1 was reached for n = 2 (Model run five; Fig. 21a), underestimating incision at Cairo (1419 m) for around 100 m, and overestimating incision at Assiut (1074 m) for around 250 m. Another model run with n = 2 but lower concavity index θ = 0.4 (Model run seven) was executed to see if a lower concavity index could compensate for this over- and underestimation but had a negligible effect (Tab. 1; results for model run seven are not shown). For the chosen erosion coefficients K, it takes 120 Kyr, 150 Kyr, 90 Kyr and 75 Kyr (model runs four to seven) respectively for significant erosion to occur at Aswan.

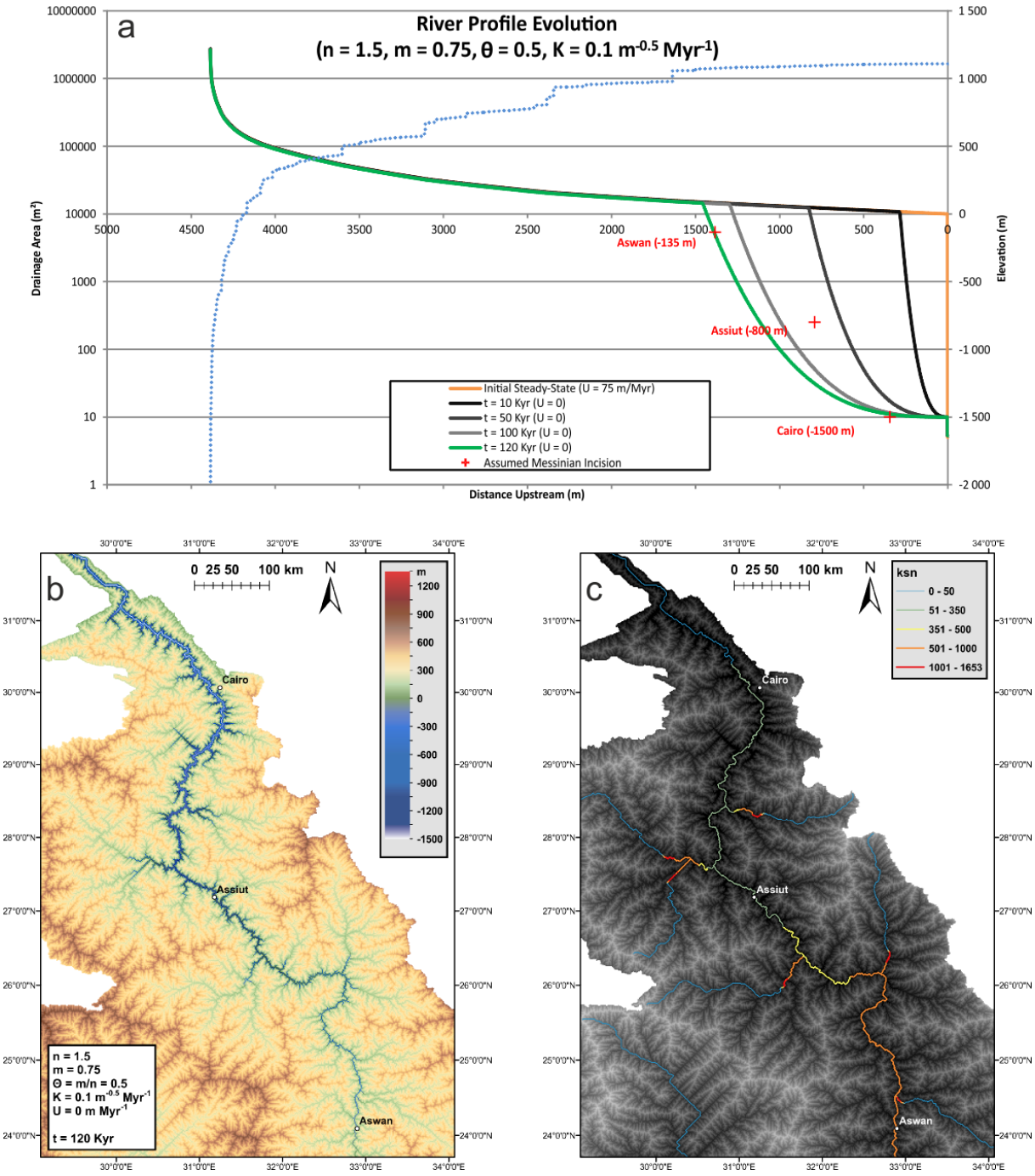

Figure 19: Results for model run four (n = 1.5). (a) The initial steep knickpoint evolves by rotating about its base. In time this leads to the formation of a slope-break knickpoint. As a whole this knickpoint does not move upstream significantly. The knickpoint lip remains sharp throughout the model run. No significant incision occurs upstream of the knickpoint lip. (b) Topographic map of the model region up to Aswan after the final modelling step, corresponding to the green river profile. (c) Map of k_{sn} values after the final modelling step. Highest k_{sn} values (and thus stream-power) correspond to the steepest part of the knickpoint, just downstream of the knickpoint lip. For further explanation of the shown river profiles and maps see Fig. 13. Model parameters for this model run can be seen in (a) and (b).

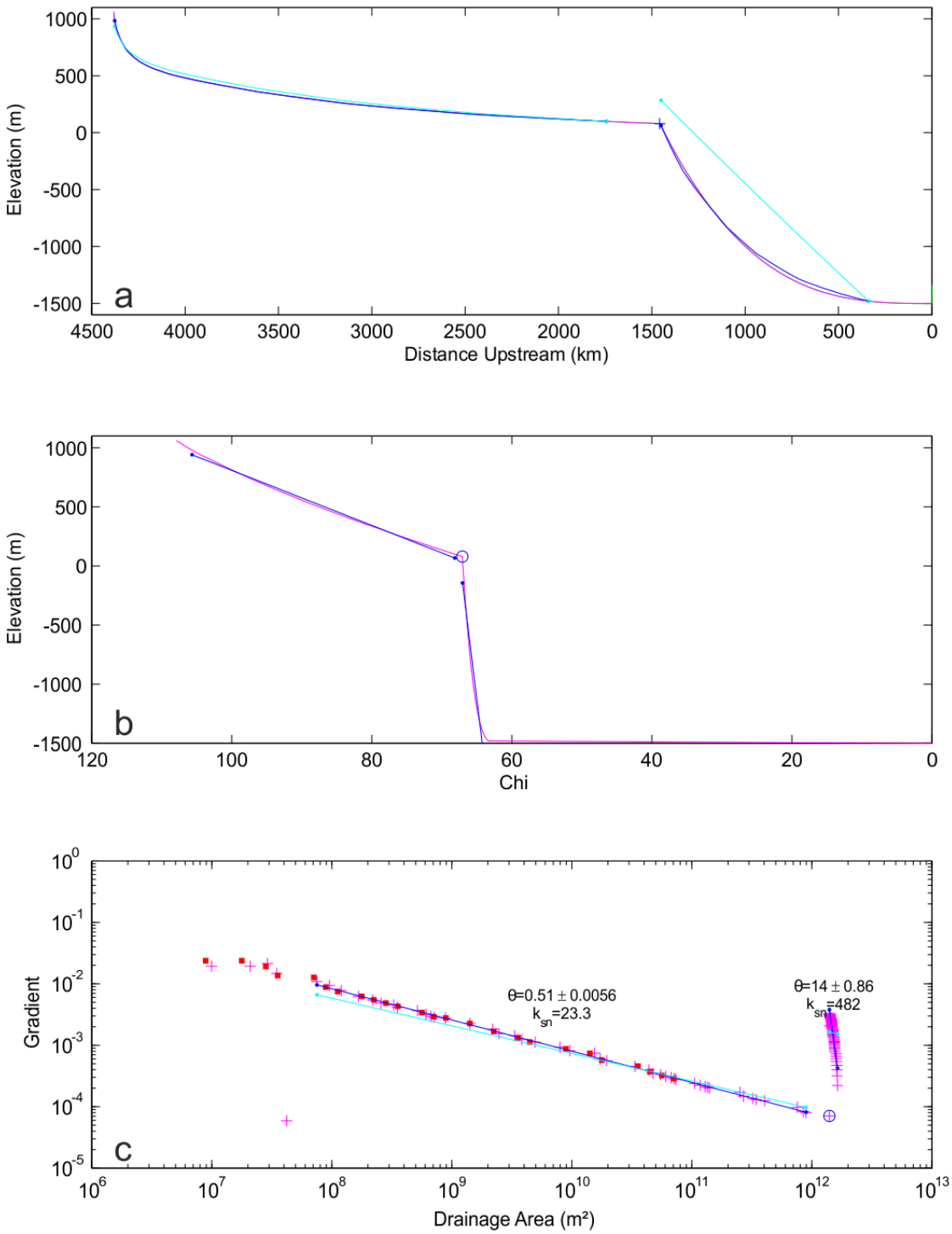

Figure 20: River profile analysis for model run foure (n = 1.5). (a) Longitudinal river profile, showing a slope-break knickpoint. (b) Chi plot showing the segmented river profile, each segment plotting as an approximately straight line, indicative for a river in steady-state, separated by a very steep part corresponding to the slope-break knickpoint. (c) Slope-area data, where the knickpoint shows as a spike with a high and positive concavity index Θ. The ancient part of the river upstream of the knickpoint shows the characteristics of the equilibrated river profile (Θ = 0.5), prior to sea-level fall. The cross in the longitudinal profile shows location of the beginning of the knickzone, corresponding to circles in second and third plot. For parameters used and further explanation (blue and cyan lines etc.) see Fig. 10.

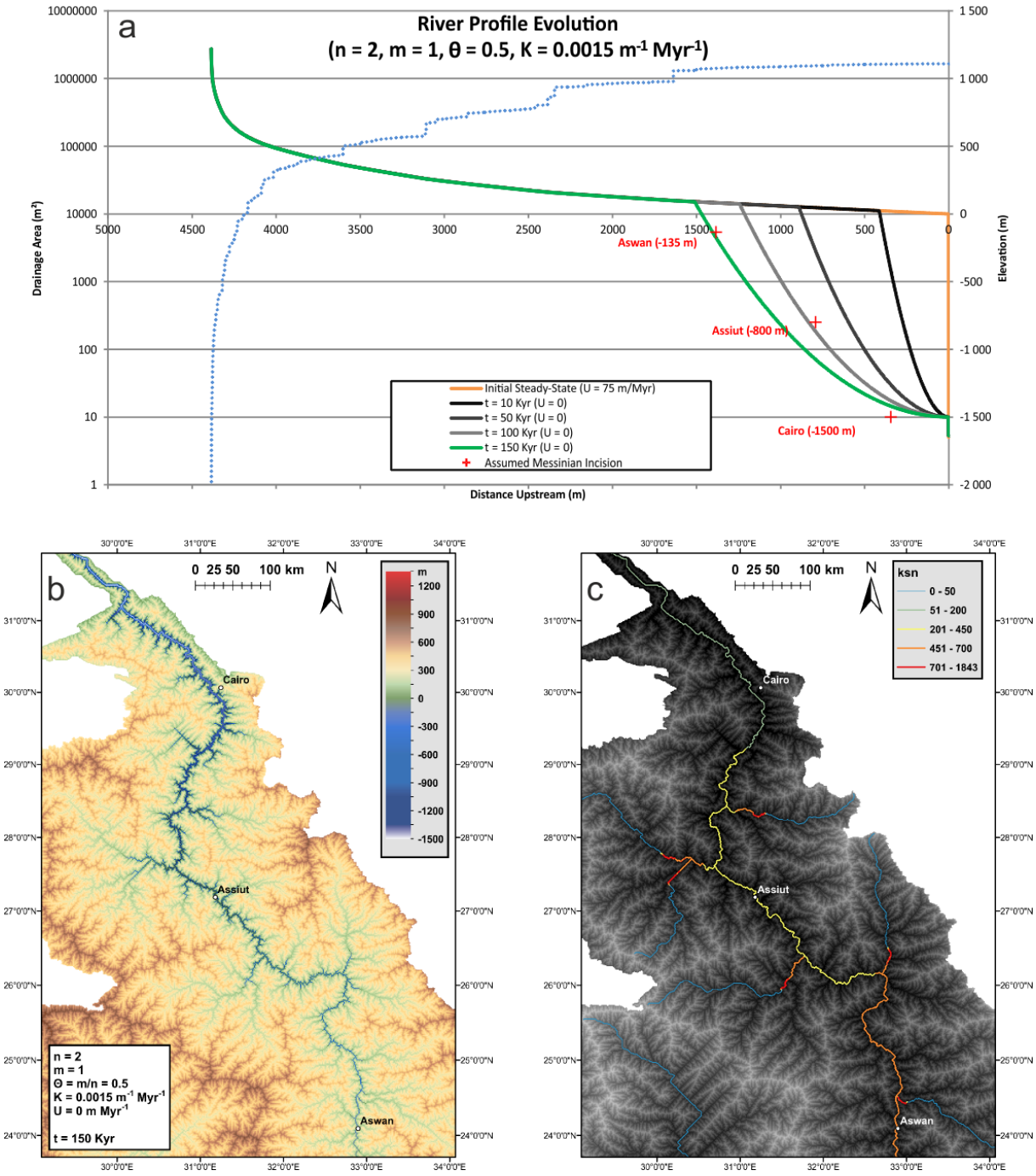

Figure 21: Results for model run five (n = 2). (a) The initial steep knickpoint evolves by rotating about its base. In time this leads to the formation of a slope-break knickpoint. As a whole this knickpoint does not move upstream significantly. The knickpoint lip remains sharp throughout the model run. No significant incision occurs upstream of the knickpoint lip. (b) Topographic map of the model region up to Aswan after the final modelling step, corresponding to the green river profile. (c) Map of k_{sn} values after the final modelling step. Highest k_{sn} values (and thus stream-power) correspond to the steepest part of the knickpoint, just downstream of the knickpoint lip. For further explanation of the shown river profiles and maps see Fig. 13. Model parameters for this model run can be seen in (a) and (b).

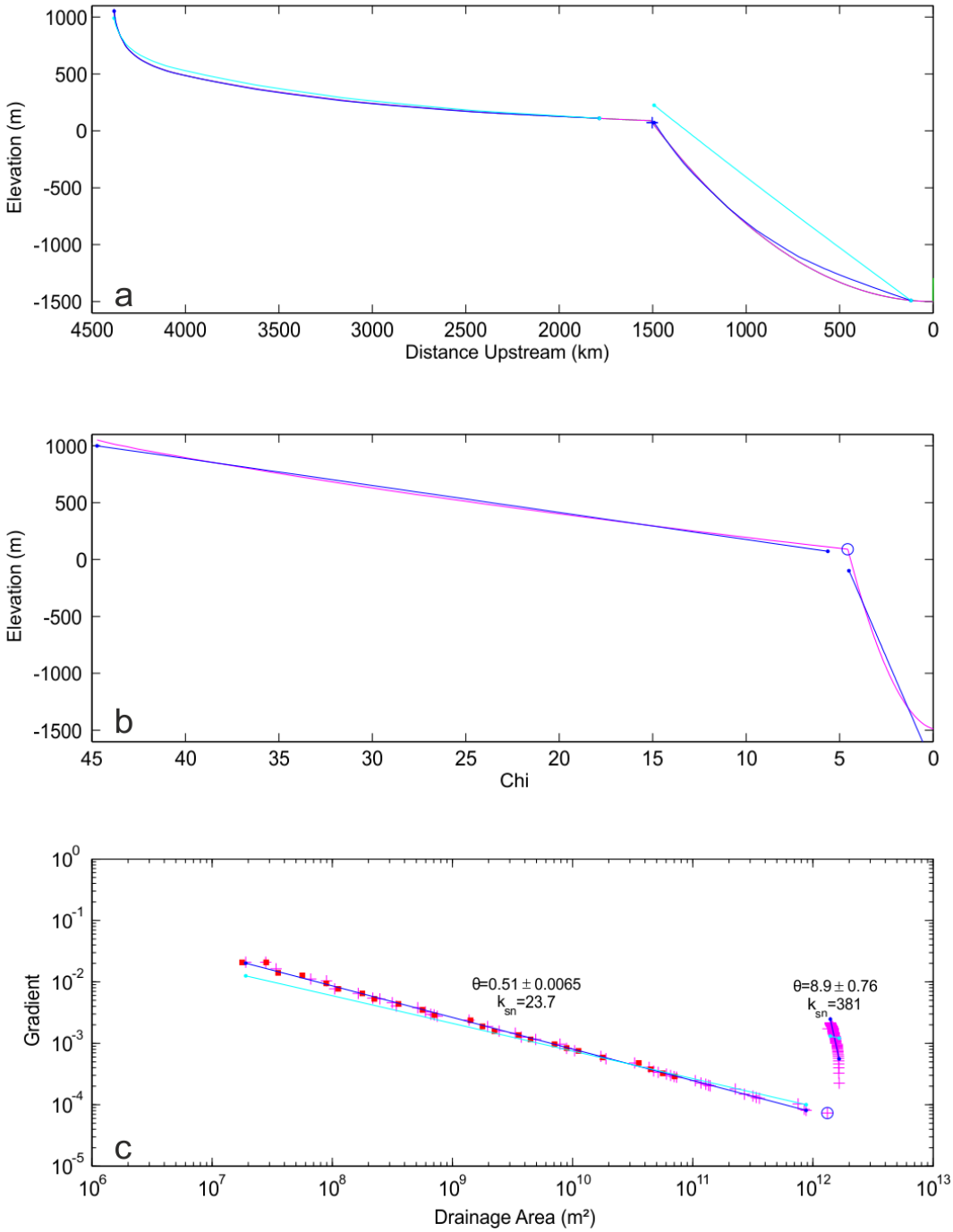

Figure 22: River profile analysis for model run five (n = 2). (a) Longitudinal river profile, showing a slope-break knickpoint. (b) Chi plot showing the segmented river profile, each segment plotting as an approximately straight line, indicative for a river in steady-state, separated by a very steep part corresponding to the slope-break knickpoint. (c) Slope-area data, where the knickpoint shows as a spike with a high and positive concavity index Θ. The ancient part of the river upstream of the knickpoint shows the characteristics of the equilibrated river profile (Θ = 0.5), prior to sea-level fall. The cross in the longitudinal profile shows location of the beginning of the knickzone, corresponding to circles in second and third plot. For parameters used and further explanation (blue and cyan lines etc.) see Fig. 10.

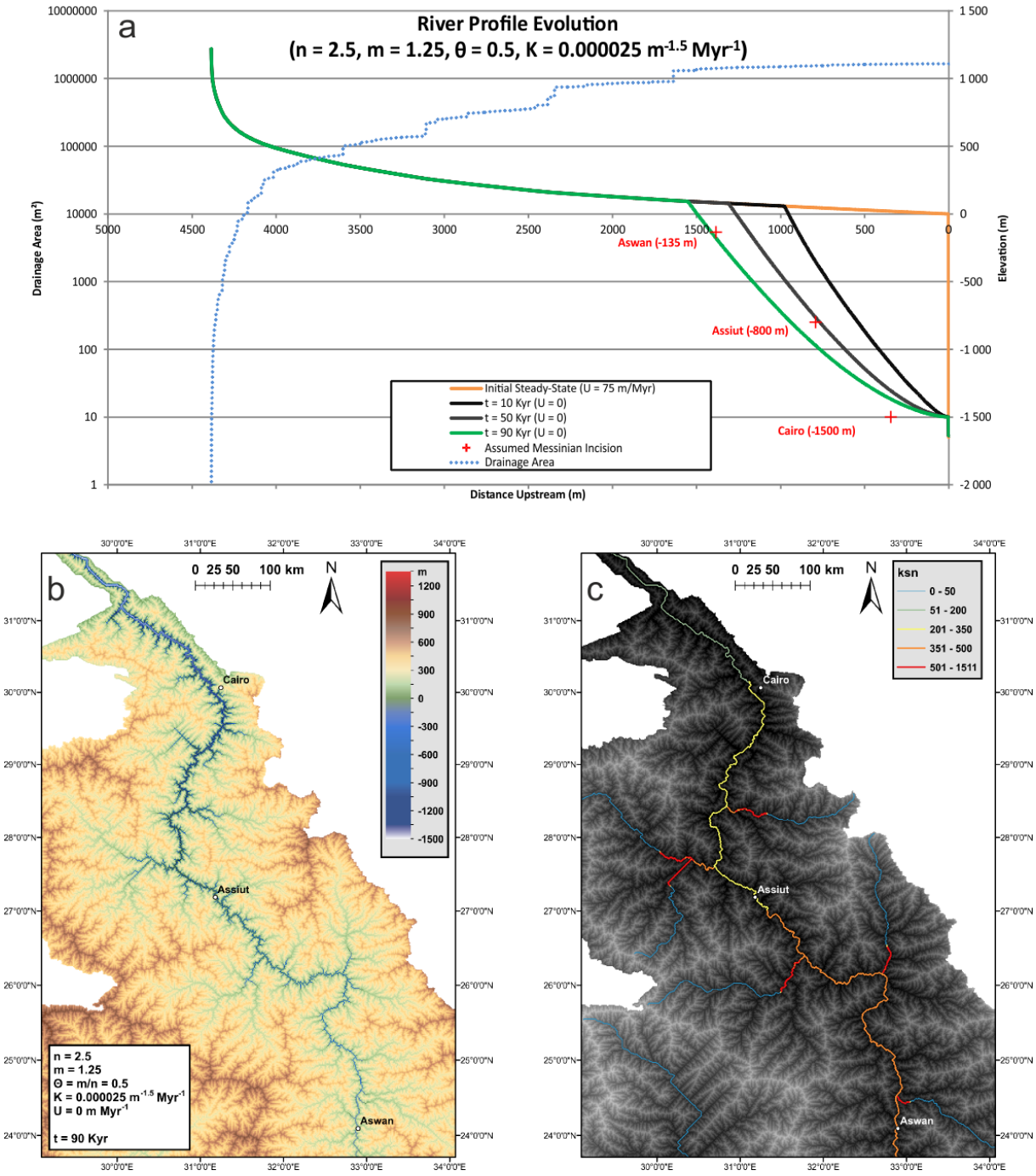

Figure 23: Results for model run six (n = 2.5). (a) The initial steep knickpoint evolves by rotating about its base. In time this leads to the formation of a slope-break knickpoint. As a whole this knickpoint does not move upstream significantly. The knickpoint lip remains sharp throughout the model run. No significant incision occurs upstream of the knickpoint lip. (b) Topographic map of the model region up to Aswan after the final modelling step, corresponding to the green river profile. (c) Map of k_{sn} values after the final modelling step. Highest k_{sn} values (and thus stream-power) correspond to the steepest part of the knickpoint, just downstream of the knickpoint lip. For further explanation of the shown river profiles and maps see Fig. 13. Model parameters for this model run can be seen in (a) and (b).

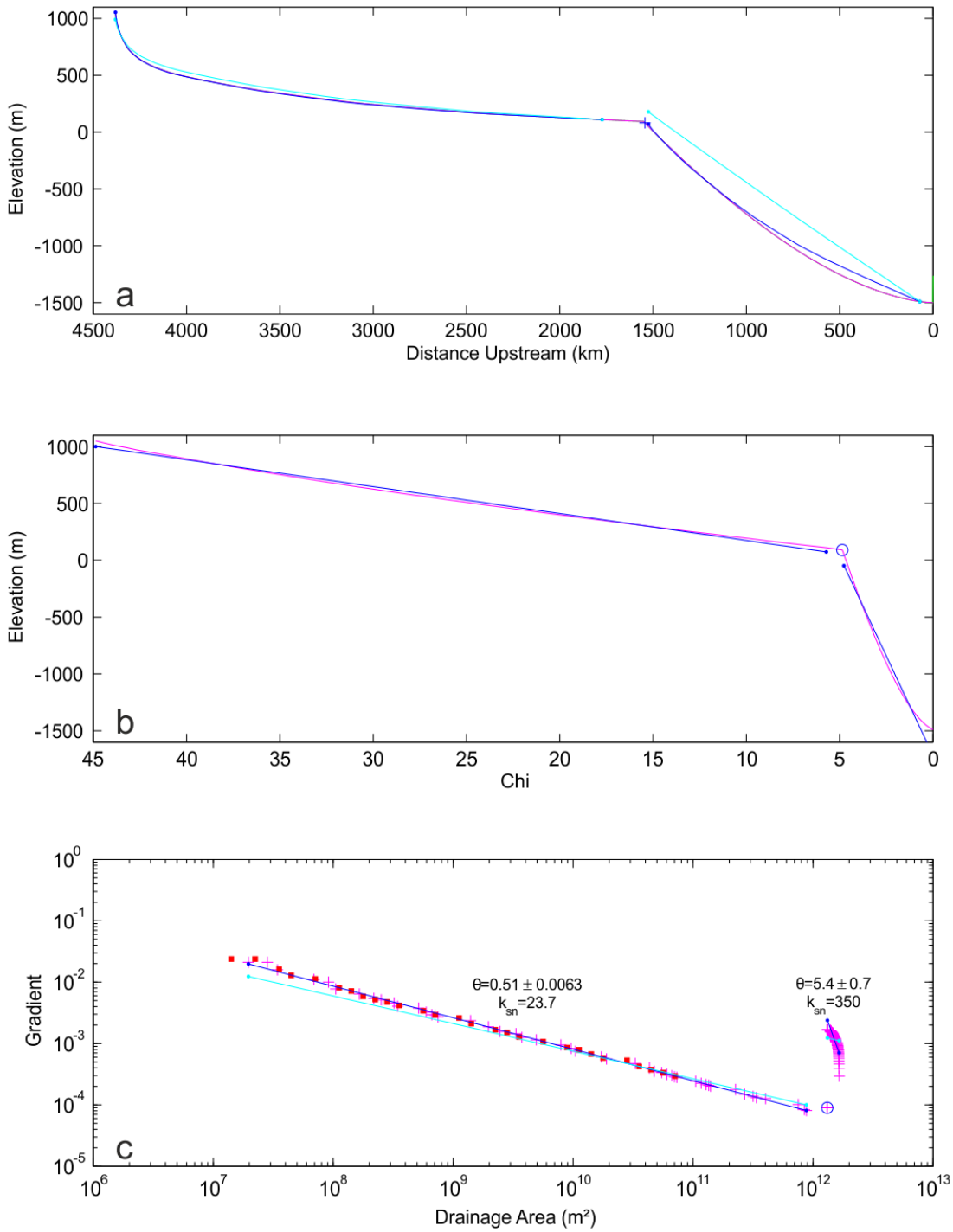

Figure 24: River profile analysis for model run six (n = 2.5). (a) Longitudinal river profile, showing a slope-break knickpoint. (b) Chi plot showing the segmented river profile, each segment plotting as an approximately straight line, indicative for a river in steady-state, separated by a very steep part corresponding to the slope-break knickpoint. (c) Slope-area data, where the knickpoint shows as a spike with a high and positive concavity index Θ. The ancient part of the river upstream of the knickpoint shows the characteristics of the equilibrated river profile (Θ = 0.5), prior to sea-level fall. The cross in the longitudinal profile shows location of the beginning of the knickzone, corresponding to circles in second and third plot. For parameters used and further explanation (blue and cyan lines etc.) see Fig. 10.

7. Discussion

For the linear SPIM with n = 1 knickpoints evolve by parallel retreat (Fig. 6b; Gardner, 1983). This cannot reproduce the expected Messinian river profile which needs a flatter gradient between Assiut and Cairo. However a linear SPIM has been used successfully to estimate knickpoint migration rates, where the knickpoint geometry was neglected (e.g., Berlin and Anderson, 2007; Crosby and Whipple, 2006; Loget and Van Den Driessche, 2009). For n = 1 (Model run one) a better constrained erosion coefficient with $K = 10^{-5}$ yr^{-1} was found using the study of Loget and Van Den Driessche (2009). They examined the rate of knickpoint migration using Messinian knickpoints, especially the ones of the Messinian Rhone and Nile rivers. Using a knickpoint celerity equation in the form of equation (13), assuming n = 1, they propose a value of m = 0.5 and therefore θ = 0.5 for Messinian knickpoints. Depending on the duration of the erosional phase (90 Kyr to 300 Kyr) and the length of the Messinian incision (1000 km to 2000 km) they estimate migration rates of 3.3 m yr^{-1} to 20 m yr^{-1} for the Messinian Nile knickpoint. This results in an erosion coefficient K of ~6 * 10^{-6} yr^{-1} for the Messinian Nile, assuming that the Messinian Nile drainage area was similar to the present day drainage area, as was done in their study. They further state that the erosion coefficient should lie around 10^{-5} yr^{-1}, and given that the estimated Messinian drainage area used in this thesis is lower than present day drainage area, a value of $K = 10^{-5}$ yr^{-1} = 10 Myr^{-1} was used for the linear SPIM. The same value for K for the same exponents of n and m was also used by Tucker and Whipple (2002). Using this erosion coefficient the knickpoint needs 105 Kyr to reach Aswan, 1384 km upstream of its point of initiation, leading to an average migration rate of C ~ 13 m yr^{-1}. This is a higher migration rate than modern migration rates for rivers with similar drainage area (see Tab. 2 in Loget and Van Den Driessche, 2009). As the time span for the cutting of the Messinian canyons is thought to be between 90 Kyr and 300 Kyr, the estimated migration rate for 105 Kyr forms the upper boundary. But even if the migration rate is cut down to a third (~4.3 m yr^{-1} for ~300 Kyr) its higher than the ones observed today. The proposed wetter climate in North Africa during the Messinian (Griffin, 2002) could account for the higher migration rate as climate and precipitation influence the erosion coefficient K. Therefore an erosion coefficient around $K = 10^{-5}$ yr^{-1} seems plausible for the Messinian Nile river.

For the case of $n > 1$, the knickpoint evolves by inclination, by simply rotating about its initial point at the knickpoint face (Fig. 6b; Gardner, 1983). A sea-level fall of 1500 m is not sufficient to generate the 1500 m incision expected at Cairo and overestimates the incision at Assiut. The underestimation of incision at Cairo could be compensated by a higher sea-level fall, probably around 1600 m. Although this would still be a valid assumption for the magnitude of Messinian sea-level fall it would not lead to a better fit of the Messinian river profile, as it would even further overestimate the incision at Assiut.

For the case of $n < 1$ the knickpoint evolves by replacement (Fig. 6b; Gardner, 1983). A simple SPIM with $n = 0.75$, $m = 0.3$ and $\theta = 0.4$ (Model run three) is able to reproduce the expected Messinian river profile. With the chosen erodibility K it takes the river 77 Kyr to reach the expected incision at Aswan, which is below the lower boundary for the duration of the sea-level low-stand of 90 Kyr. This could be corrected by choosing a slightly lower erodibility K. Outside of the Messinian Nile channel decay of the topography below modern day sea-level is observed, an unrealistic scenario for the Messinian. This could be due to the high erodibility K being uniform over the whole model region, so that its value might be plausible for the Nile channel but not for the rest of the region. This high value of K also leads to significant incision for the Messinian Nile river upstream of the knickpoint. One reason for a higher K value within the channel could be the channelization of the flow due to decrease in channel width in response to the incision, as channel width also influences K. In the simple SPIM used, channel width is thought to increase with increase in drainage area, which would not be true for the Messinian knickpoint. Also the chosen erosion model and its parameters could simply only be true for the Nile channel, for which the results seem appropriate, but not for the rest of the model region. Outside of the channel other processes and/or erosion mechanism, not even considered in these model runs, are likely at work.

Values of $n \sim 0.7$ and $m \sim 0.3$ relate to erosion models where bedrock incision is proportional to shear stress rather than stream-power and where plucking is probably the main erosion mechanism (Bishop et al., 2005; Howard et al., 1994; Whipple et al., 2000). These values lead to evolution of the knickpoint by replacement, which is the expected evolution for vertical knickpoints in most cases (Gardner, 1983). Using values of $n < 1$ and $\theta = 0.4$ Royden and Perron (2013) were also able to produce

good fits for their modelling of the Rio Torto river. The observed incision upstream of the actual knickzone is consistent with the observation made by Berlin and Anderson (2009) of enhanced incision and channel steepening due to flow acceleration above waterfalls. The evolution of the knickpoint in this detachment-limited erosion model shows a diffusional behaviour. Diffusive like behaviour was also observed in the modelling of the Messinian Rhone profile by Loget et al. (2006), although they did not use a stream-power erosion model. For the modelling of post-glacial gorge incision by Valla et al. (2010) a detachment-limited model alone was not able to model the observed transient evolution which also showed diffusional behaviour, even though they tested values of $n < 1$ to allow for some knickpoint lip diffusion. Knickpoints in their study evolved through a “replacement-like” dynamic, with fluvial abrasion probably being the main incision process. They conclude that long-term evolution of bedrock gorges cannot be caused by detachment-limited mechanisms alone, as sediment supply and transport, as well as evolving channel geometry, play an import role during long-term gorge incision. They were able to produce better results with a simple transport-limited model.

Regarding the absolute time within all of these river profiles and the associated migration rates one has to be careful. First, the value of K is only loosely constrained but has great influence on migration rate. In this thesis the value of K was not chosen due to observations of lithology, climate, etc., but to allow incision up to Aswan within around 100 Kyr. Erosion coefficient K is also kept constant in space and time for the whole model run, a very simplistic view. Still, the used erosion coefficient $K = 10^{-5}$ yr^{-1} for the linear model run with $n = 1$ is probably a good indicator and the actual erosion coefficient should lay somewhere near that value. However, for the non-linear case of $n \neq 1$ migration rate depends on slope S. This in combination with incision being calculated explicitly for $n \neq 1$ makes migration rates also sensitive to the chosen time step dt. For all model runs with $n \neq 1$ migration slows down with time, as would be expected when the initial steep (vertical) knickpoint gets flatter and upstream drainage area decreases. However, the higher the time step dt, the longer the time in which the knickpoint migrates according to the initial near vertical slope for the first time step. This is also true for all the successive erosional steps, although this effect is greatest for the first one. Due to these two reasons although for all model runs with $n \neq 1$ values for K and t are assigned, both of this estimated values should be regarded as only very rough estimates.

8. Conclusion

The conclusion of this thesis is that a simple stream-power erosion model with n = 0.75, m = 0.3 and θ = 0.4 with a sea-level fall of 1500 m is able to reproduce the expected incision depth of the Messinian Nile river at Cairo, Assiut and Aswan. These set of parameter values and the corresponding observations in the evolution of the river profile are consistent with the results of other modelling studies in the literature. But slope exponent n is also often assumed to be greater than unity and long-term values of $n > 2$ are also to be expected. Using a value of n = 2, m = 1 and θ = 0.5 the observed incision could only be partly reproduced. However, including a possible isostatic response of the continental margin due to loading and unloading of the Mediterranean, adding a pattern of precipitation to the model region, a two-step sea-level fall, or the inclusion of the tools and cover effect and a threshold term in the stream-power model could allow for other model parameters to also fit the observed incision. Further, the observed diffusional behaviour would suggest that a transport-limited or hybrid erosion model may also be able to produce the expected river profile. More modelling runs, using different erosion models and including the factors mentioned, would thus lead to a better understanding of the erosion dynamics associated with the cutting of the Messinian canyon.

References

Abdelkareem, M., Ghoneim, E., El-Baz, F., Askalany, M., 2012. New insight on paleoriver development in the Nile basin of the eastern Sahara. Journal of African Earth Sciences 62, 35-40.

Abotalib, A.Z., Mohamed, Ramadan S. A., 2013. Surface evidences supporting a probable new concept for the river systems evolution in Egypt: a remote sensing overview. Environ Earth Sci 69, 1621-1635.

Barber, P.M., 1981. Messinian subaerial erosion of the proto-Nile Delta. Marine Geology 44, 253-272.

Barry, R.G., Chorley, R.J., 2010. Atmosphere, weather and climate. Routledge, London.

Berlin, M.M., Anderson, R.S., 2007. Modeling of knickpoint retreat on the Roan Plateau, western Colorado. J. Geophys. Res. 112, 1-16.

Berlin, M.M., Anderson, R.S., 2009. Steepened channels upstream of knickpoints: Controls on relict landscape response. J. Geophys. Res. 114, 1-20.

Bini, A., Cita, M.B., Gaetani, M., 1978. Southern Alpine lakes — Hypothesis of an erosional origin related to the Messinian entrenchment. Marine Geology 27, 271-288.

Bishop, P., Hoey, T.B., Jansen, J.D., Artza, I.L., 2005. Knickpoint recession rate and catchment area: the case of uplifted rivers in Eastern Scotland. Earth Surf. Process. Landforms 30, 767-778.

Chumakov, I.S., 1973. Geological History of the Mediterranean at the End of the Miocene - the Beginning of the Pliocene According to New Data. In: Ryan, W.B.F., Hsu, K. (Eds.), Initial Reports of the Deep Sea Drilling Project, 13. U.S. Government Printing Office.

Clauzon, G., 1978. The Messinian Var canyon (Provence, southern France) — Paleogeographic implications. Marine Geology 27, 231-246.

Clauzon, G., 1982. Le canyon messinien du Rhone; une preuve decive du "desiccated deep-basin model" (Hsue, Cita and Ryan, 1973). Bulletin de la Societe Geologique de France S7-XXIV, 597-610.

Clauzon, G., Suc, J.-P., Gautier, F., Berger, A., Loutre, M.-F., 1996. Alternate interpretation of the Messinian salinity crisis: Controversy resolved? Geol 24, 363.

Crosby, B.T., Whipple, K.X., 2006. Knickpoint initiation and distribution within fluvial networks: 236 waterfalls in the Waipaoa River, North Island, New Zealand. Geomorphology 82, 16-38.

Duggen, S., Hoernle, K., van den Bogaard, Paul, Rüpke, L., Morgan, J.P., 2003. Deep roots of the Messinian salinity crisis. Nature 422, 602-606.

El Mahmoudi, A., Gabr, A., 2009. Geophysical surveys to investigate the relation between the Quaternary Nile channels and the Messinian Nile canyon at East Nile Delta, Egypt. Arab J Geosci 2, 53-67.

El-Sayed, A., Vaccari, F., Panza, G.F., 2004. The Nile Valley of Egypt: A Major Active Graben that Magnifies Seismic Waves. Pure and Applied Geophysics 161, 983-1002.

Finckh, P.G., 1978. Are southern Alpine lakes former Messinian canyons? — Geophysical evidence for preglacial erosion in the southern Alpine lakes. Marine Geology 27, 289-302.

Flint, J.J., 1974. Stream gradient as a function of order, magnitude, and discharge. Water Resour. Res. 10, 969-973.

Frankel, K.L., Pazzaglia, F.J., Vaughn, J.D., 2007. Knickpoint evolution in a vertically bedded substrate, upstream-dipping terraces, and Atlantic slope bedrock channels. Geol Soc America Bull 119, 476-486.

Garcia-Castellanos, D., Villaseñor, A., 2011. Messinian salinity crisis regulated by competing tectonics and erosion at the Gibraltar arc. Nature 480, 359-363.

Gardner, T.W., 1983. Experimental study of knickpoint and longitudinal profile evolution in cohesive, homogeneous material. Geol Soc America Bull 94, 664-672.

Gargani, J., 2004. Modelling of the erosion in the Rhone valley during the Messinian crisis (France). Quaternary International 121, 13-22.

Gargani, J., Bache, F., Jouannic, G., Gorini, C., 2014. Slope destabilization during the Messinian Salinity Crisis. Geomorphology 213, 128-138.

Gargani, J., Rigollet, C., 2007. Mediterranean Sea level variations during the Messinian salinity crisis. Geophys. Res. Lett. 34, 253.

Gargani, J., Rigollet, C., Scarselli, S., 2010. Isostatic response and geomorphological evolution of the Nile valley during the Messinian salinity crisis. Bulletin de la Societe Geologique de France 181, 19-26.

Gaullier, V., Loncke, L., Vendeville, B., Déverchère, J., Droz, L., Obone Zue Obame, E.M., Mascle, J., 2008. The Messinian Salinity Crisis from Mega-deposits to Microbiology - A Consensus Report, 91-96.

Gilbert, G.K., 1877. Report on geology of Henry Mountains. U.S. G.P.O., Washington, D.C.

Gladstone, R., Flecker, R., Valdes, P., Lunt, D., Markwick, P., 2007. The Mediterranean hydrologic budget from a Late Miocene global climate simulation. Palaeogeography, Palaeoclimatology, Palaeoecology 251, 254-267.

Goudie, A.S., 2005. The drainage of Africa since the Cretaceous. Geomorphology 67, 437-456.

Govers, R., Meijer, P., Krijgsman, W., 2009. Regional isostatic response to Messinian Salinity Crisis events. Tectonophysics 463, 109-129.

Grant, G.E., O'Connor, J.E., Wolman, M.G., 2013. 9.2 A River Runs Through It: Conceptual Models in Fluvial Geomorphology. In: Treatise on Geomorphology. Elsevier, pp. 6-21.

Griffin, D.L., 1999. The late Miocene climate of northeastern Africa: unravelling the signals in the sedimentary succession. Journal of the Geological Society 156, 817-826.

Griffin, D.L., 2002. Aridity and humidity: two aspects of the late Miocene climate of North Africa and the Mediterranean. Palaeogeography, Palaeoclimatology, Palaeoecology 182, 65-91.

Hack, J.T., 1957. Studies of longitudinal stream profiles in Virginia and Maryland. U.S. Govt. Print. Off., Washington.

Harel, M.-A., Mudd, S.M., Attal, M., 2016. Global analysis of the stream power law parameters based on worldwide 10 Be denudation rates. Geomorphology 268, 184-196.

Harkins, N., Kirby, E., Heimsath, A., Robinson, R., Reiser, U., 2007. Transient fluvial incision in the headwaters of the Yellow River, northeastern Tibet, China. J. Geophys. Res. 112, 1-21.

Haviv, I., Enzel, Y., Whipple, K.X., Zilberman, E., Matmon, A., Stone, J., Fifield, K.L., 2010. Evolution of vertical knickpoints (waterfalls) with resistant caprock: Insights from numerical modeling. J. Geophys. Res. 115, 1-22.

Howard, A., 1980. Thresholds in river regimes, 227-258.

Howard, A., 1998. Long Profile Development of Bedrock Channels: Interaction of Weathering, Mass Wasting, Bed Erosion, and Sediment Transport 107.

Howard, A.D., 1994. A detachment-limited model of drainage basin evolution. Water Resour. Res. 30, 2261-2285.

Howard, A.D., Dietrich, W.E., Seidl, M.A., 1994. Modeling fluvial erosion on regional to continental scales. J. Geophys. Res. 99, 13971-13986.

Howard, A.D., Kerby, G., 1983. Channel changes in badlands. Geol Soc America Bull 94, 739.

Hsue, K.J., Cita, M.B., 1973. The Origin of the Mediterranean Evaporite. In: Ryan, W.B.F., Hsu, K. (Eds.), Initial Reports of the Deep Sea Drilling Project, 13. U.S. Government Printing Office.

Hsue, K.J., Ryan, W. B. F., Cita, M.B., 1973. Late Miocene Desiccation of the Mediterranean. Nature 242, 240-244.

Jolivet, L., Augier, R., Robin, C., Suc, J.-P., Rouchy, J.M., 2006. Lithospheric-scale geodynamic context of the Messinian salinity crisis. Sedimentary Geology 188-189, 9-33.

Kirby, E., Whipple, K.X., 2012. Expression of active tectonics in erosional landscapes. Journal of Structural Geology 44, 54-75.

Krijgsman, W., Hilgen, F.J., Raffi, I., Sierro, F.J., Wilson, D.S., 1999. Chronology, causes and progression of the Messinian Salinity Crisis. Nature 400, 652-655.

Lague, D., 2014. The stream power river incision model: evidence, theory and beyond. Earth Surf. Process. Landforms 39.

Lamb, M.P., Dietrich, W.E., 2009. The persistence of waterfalls in fractured rock. Geol Soc America Bull 121, 1123-1134.

Loget, N., Davy, P., Van Den Driessche, J., 2006. Mesoscale fluvial erosion parameters deduced from modeling the Mediterranean sea level drop during the Messinian (late Miocene). J. Geophys. Res. Earth Surf. 111, n/a.

Loget, N., Driessche, Jean Van Den, Davy, P., 2005. How did the Messinian Salinity Crisis end? Terra Nova 17, 414-419.

Loget, N., Van Den Driessche, Jean, 2009. Wave train model for knickpoint migration. Geomorphology 106, 376-382.

Mackin, J., 1948. Concept of the Graded River. Geol Soc America Bull 59, 463.

Molnar, P., England, P., Martinod, J., 1993. Mantle dynamics, uplift of the Tibetan Plateau, and the Indian Monsoon. Rev. Geophys. 31, 357.

Montgomery, D.R., Abbe, T.B., Buffington, J.M., Peterson, N.P., Schmidt, K.M., Stock, J.D., 1996. Distribution of bedrock and alluvial channels in forested mountain drainage basins. Nature 381, 587-589.

Pelletier, J.D., 2013. 2.3 Fundamental Principles and Techniques of Landscape Evolution Modeling. In: Treatise on Geomorphology. Elsevier, pp. 29-43.

Perron, J.T., Royden, L., 2013. An integral approach to bedrock river profile analysis. Earth Surf. Process. Landforms 38, 570-576.

Roden, J., Abdelsalam, M.G., Atekwana, E., El-Qady, G., Tarabees, E.A., 2011. Structural influence on the evolution of the pre-Eonile drainage system of southern

Egypt: Insights from magnetotelluric and gravity data. Journal of African Earth Sciences 61, 358-368.

Roveri, M., Flecker, R., Krijgsman, W., Lofi, J., Lugli, S., Manzi, V., Sierro, F.J., Bertini, A., Camerlenghi, A., Lange, G. de, Govers, R., Hilgen, F.J., Hübscher, C., Meijer, P.T., Stoica, M., 2014. The Messinian Salinity Crisis: Past and future of a great challenge for marine sciences. Marine Geology 352, 25-58.

Royden, L., Taylor Perron, J., 2013. Solutions of the stream power equation and application to the evolution of river longitudinal profiles. J. Geophys. Res. Earth Surf. 118, 497-518.

Ryan, W.B.F., 2009. Decoding the Mediterranean salinity crisis. Sedimentology 56, 95-136.

Said, R., 1981. The geological evolution of the river Nile. Springer New York, New York, NY.

Said, R., 1994. The river Nile. Geology, hydrology, and utilization. Pergamon, Oxford [England], New York.

Schumm, S.A., 1993. River Response to Baselevel Change: Implications for Sequence Stratigraphy. The Journal of Geology 101, 279-294.

Sklar, L.S., Dietrich, W.E., 2004. A mechanistic model for river incision into bedrock by saltating bed load. Water Resour. Res. 40, 225.

Snyder, N.P., Whipple, K.X., Tucker, G.E., Merritts, D.J., 2000. Landscape response to tectonic forcing: Digital elevation model analysis of stream profiles in the Mendocino triple junction region, northern California. Geological Society of America Bulletin 112, 1250-1263.

Stock, J.D., Montgomery, D.R., 1999. Geologic constraints on bedrock river incision using the stream power law. J. Geophys. Res. 104, 4983-4993.

Thurmond, A.K., Stern, R.J., Abdelsalam, M.G., Nielsen, K.C., Abdeen, M.M., Hinz, E., 2004. The Nubian Swell. Journal of African Earth Sciences 39, 401-407.

Tucker, G.E., Hancock, G.R., 2010. Modelling landscape evolution. Earth Surf. Process. Landforms 35, 28-50.

Tucker, G.E., Whipple, K.X., 2002. Topographic outcomes predicted by stream erosion models: Sensitivity analysis and intermodel comparison. J. Geophys. Res. 107, ETG 1-1.

Valla, P.G., van der Beek, Peter A., Lague, D., 2010. Fluvial incision into bedrock: Insights from morphometric analysis and numerical modeling of gorges incising glacial hanging valleys (Western Alps, France). J. Geophys. Res. Earth Surf. 115, n/a.

Whipple, K.X., 2004. Bedrock rivers and the geomorphology of active orogens. Annu. Rev. Earth Planet. Sci. 32, 151-185.

Whipple, K.X., DiBiase, R.A., Crosby, B.T., 2013. 9.28 Bedrock Rivers. In: Treatise on Geomorphology. Elsevier, pp. 550-573.

Whipple, K.X., Hancock, G.S., Anderson, R.S., 2000. River incision into bedrock: Mechanics and relative efficacy of plucking, abrasion, and cavitation. Geological Society of America Bulletin 112, 490-503.

Whipple, K.X., Tucker, G.E., 1999. Dynamics of the stream-power river incision model: Implications for height limits of mountain ranges, landscape response timescales, and research needs. J. Geophys. Res. 104, 17661-17674.

Whipple, K.X., Tucker, G.E., 2002. Implications of sediment-flux-dependent river incision models for landscape evolution. J. Geophys. Res. 107, 453.

Wobus, C.W., Crosby, B.T., Whipple, K.X., 2006. Hanging valleys in fluvial systems: Controls on occurrence and implications for landscape evolution. J. Geophys. Res. 111, 767.

Woodward, J.C., Macklin, M.G., Krom, M.D., Williams, M.A.J., 2007. The Nile: Evolution, Quaternary River Environments and Material Fluxes. In: Gupta, A. (Ed.), Large Rivers. John Wiley & Sons, Ltd, Chichester, UK, pp. 261-292.

Zachos, J., Pagani, M., Sloan, L., Thomas, E., Billups, K., 2001. Trends, rhythms, and aberrations in global climate 65 Ma to present. Science (New York, N.Y.) 292, 686-693.

Zachos, J.C., Dickens, G.R., Zeebe, R.E., 2008. An early Cenozoic perspective on greenhouse warming and carbon-cycle dynamics. Nature 451, 279-283.

Zaki, R., 2007. Pleistocene evolution of the Nile Valley in northern Upper Egypt. Quaternary Science Reviews 26, 2883-2896.

Acknowledgements

I want to thank my supervisor Univ.-Prof. Dr. Kurt Stüwe. First for helping me to define the topic and scope of my master thesis. Further he allowed me much freedom in the realization of the thesis but at the same time he was anxious to keep the scope within manageable boundaries. During this process he was always happy to give valuable input and advise.

I also want to thank Dr. Stefan Hergarten, a former teacher at the University of Graz, now teaching at the University of Freiburg. He allowed me the usage of his OpenLEM software for my landscape evolution modelling. During the process he not only provided me with updated versions of the software but also took the time to answer all of my questions related to the software.

Finally many thanks to my family for all the support they showed during my study.